Coordination Chemistry Reviews 521 (2024) 216145

Contents lists available at ScienceDirect

Coordination Chemistry Reviews

journal homepage: www.elsevier.com/locate/ccr

Transition metal phosphides as noble-metal-alternative co-catalysts for solar hydrogen production

Tingting Liu [a,b,c], Chen Chen [a], Sixiang Liu [c], Zhangsen Chen [c], Zonghua Pu [a,*], Qiufeng Huang [a], Lei Zhang [d,*], Abdullah M. Al-Enizi [e,*], Ayman Nafady [e], Shuhui Sun [c,*], Gaixia Zhang [b,*]

[a] Fujian Key Laboratory of Polymer Materials, College of Chemistry and Materials Science, Fujian Normal University, Fuzhou, Fujian, 350007, China
[b] Department of Electrical Engineering, École de Technologie Supérieure (ÉTS), Montréal, Québec H3C 1K3, Canada
[c] Institut National de la Recherche Scientifique (INRS), Centre Énergie Matériaux Télécommunications, Varennes, Québec J3X 1P7, Canada
[d] Clean Energy Innovation (CEI) Research Center, National Research Council of Canada, Vancouver, BC V6T 1W5, Canada
[e] Department of Chemistry, College of Science, King Saud University, Riyadh 11451, Saudi Arabia

ARTICLE INFO

Keywords:
Transition-metal phosphides
Semiconductors
Visible light activity
Photocatalytic H_2 production
Water splitting

ABSTRACT

Hydrogen (H_2) emerges as a highly promising contender for replacing conventional fossil fuels due to its high combustion heat value and net-zero greenhouse gas emission. Photocatalytic H_2 generation through semiconductor-based water splitting represents a clean and sustainable technology in the field. Developing highly efficient and abundant source semiconductor materials, along with co-catalysts, is paramount in achieving the industrial-level H_2 evolution by photocatalysis technology. In recent years, transition-metal phosphides (TMPs) have emerged as powerful co-catalysts for photocatalytic reactions due to their cost-effectiveness, abundant reserves in the earth's crust, and favorable physicochemical properties, thus offering a viable alternative to conventional precious metal materials. In this review, we first provide a concise historical overview and outline the structure of TMPs. The synthetic strategies of TMPs are subsequently systematically analyzed based on diverse phosphorus sources. Additionally, this review provides a comprehensive summary of the recent research endeavors conducted on TMPs as potential photocatalytic co-catalysts for efficient hydrogen generation through photocatalysis. Eventually, this review briefly addresses the prevailing key concerns, proposed countermeasures, and forthcoming challenges associated with enhancing the efficiency of photocatalytic H_2 evolution in TMPs.

1. Introduction

Hydrogen (H_2), as an energy carrier, is considered a genuine alternative to conventional fuels (e.g., coal, gasoline, methane, etc.) due to its renewable nature, high energy output, and eco-friendly attributes [1,2]. It is expected that realizing H_2 economy will generate a high request for efficient and sustainable H_2 generation methods. Photocatalysis H_2 generation, involving the splitting of water using sunlight and photocatalysts, has emerged as a promising approach for achieving solar-driven H_2 production over the past few decades. Fujishima and colleagues reported the first demonstration of a photoelectrochemical water splitting system, which employs a rutile photoanode and a platinum (Pt) cathode for H_2 evolution in 1972 [3]. Since then, the utilization of solar energy for H_2O splitting has garnered significant attention as a potential strategy to convert solar energy into chemical energy in the form of environmentally friendly and sustainable H_2 fuel. Typically, the mechanism for photocatalytic H_2 production (Eq. (4)) employing an appropriate semiconductor is depicted in Fig. 1a [4]. It mainly follows three steps: (i) the semiconductor photocatalyst absorbs the light energy; (ii) upon solar excitation, photo-induced holes (h^+) and electrons (e^-) are generated in the valance band (VB) and conduction band (CB) of the photocatalyst, respectively (Eq. (1)); (iii) after traveling to the catalyst surface, the photo-generated holes oxidize the water into O_2 and H^+ (Eq. (2)), while photo-generated electrons reduce H^+ to H_2 (Eq. (3)).

$$2\gamma \rightarrow 2e_{CB}^{-} + 2e_{hv} + \text{photo} - \text{induced holes and electrons} \quad (1)$$

$$2H_2O + 4\,h^+ \rightarrow O_2 + 4H^+ \text{ Oxygen evolution reaction } E^o{}_{OX} = -1.23 \text{ eV} \quad (2)$$

* Corresponding authors.
E-mail addresses: zonghua.pu@fjnu.edu.cn (Z. Pu), Lei.Zhang@nrc-cnrc.gc.ca (L. Zhang), shuhui.sun@inrs.ca (S. Sun), gaixia.zhang@etsmtl.ca (G. Zhang).

https://doi.org/10.1016/j.ccr.2024.216145
Received 8 April 2024; Received in revised form 7 June 2024; Accepted 6 August 2024
Available online 25 August 2024

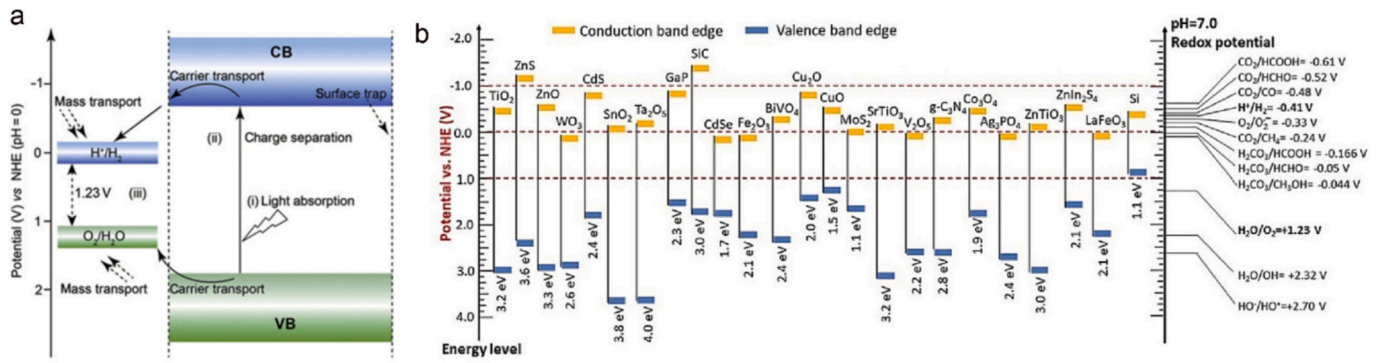

Fig. 1. (a) Schematic representation of the principal processes involved in photocatalytic H_2O splitting over a semiconductor material. Reproduced with permission from ref. 4. (b) The band structure of diverse semiconductor materials and the redox potential of various reactions. Reproduced with permission from ref. 10.

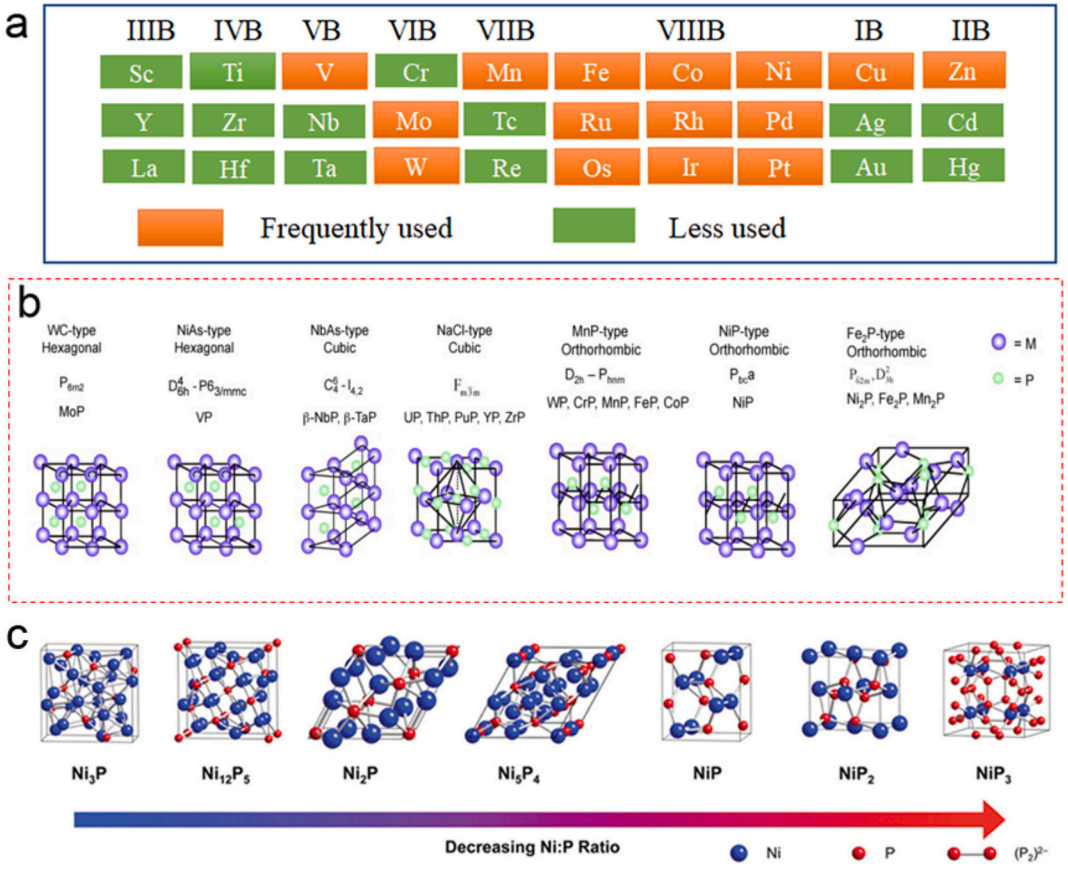

Fig. 2. (a) Elements that are used to form TMPs for electrocatalysis. (b) Typical crystal structures of TMPs. Reproduced with permission from ref. 47. (c) Crystal structures of diverse nickel phosphides. Reproduced with permission from ref. 50.

$$4H^+ + 4e^- \rightarrow H_2 \text{ Hydrogen evolution reaction } E^o_{Red} = 0 \text{ eV} \quad (3)$$

$$2H_2O + 2\gamma \rightarrow 2H_2 + O_2 \text{ Overall water splitting } \Delta E^o = 1.23 \text{ eV} \quad (4)$$

Until now, a plethora of semiconductor-based photocatalytic materials has been developed to achieve efficient catalytic H_2 generation under solar irradiation, including metal oxides (such as ZnO, WO_3, Cu_2O, FeO), metal chalcogenides (such as CdS, CdSe, ZnS_2), metal nitrides (such as GaN, InN), carbon nitrides (such as C_3N_4), metal halide perovskite (such as $CsPbBr_3$), organic materials, and metal–organic frameworks (MOFs) [5–9]. The semiconductors depicted in Fig. 1b exemplify some typical applications of different semiconductor materials with different band structures [10]. Nowadays, most semiconductors exhibit limited photocatalytic activity and stability owing to the rapid recombination of electron–hole pairs and the susceptibility to photocorrosion. On one hand, the incorporation of a sacrificial agent as an electron donor into the reaction system can effectively scavenge the photogenerated holes and suppress the oxidation of the semiconductor. On the other hand, the deposition of co-catalysts onto semiconductors can effectively mitigate the recombination rate of e^--h^+ pairs [11], thereby significantly augmenting the photocatalytic performance. By virtue of their higher work function, which corresponds to a lower Fermi level, precious-metal co-catalysts can effectively capture photoexcited electrons when combined with conventional semiconductor photocatalysts, thereby mitigating the recombination of electron-hole pairs. For example, Pt, palladium (Pd),

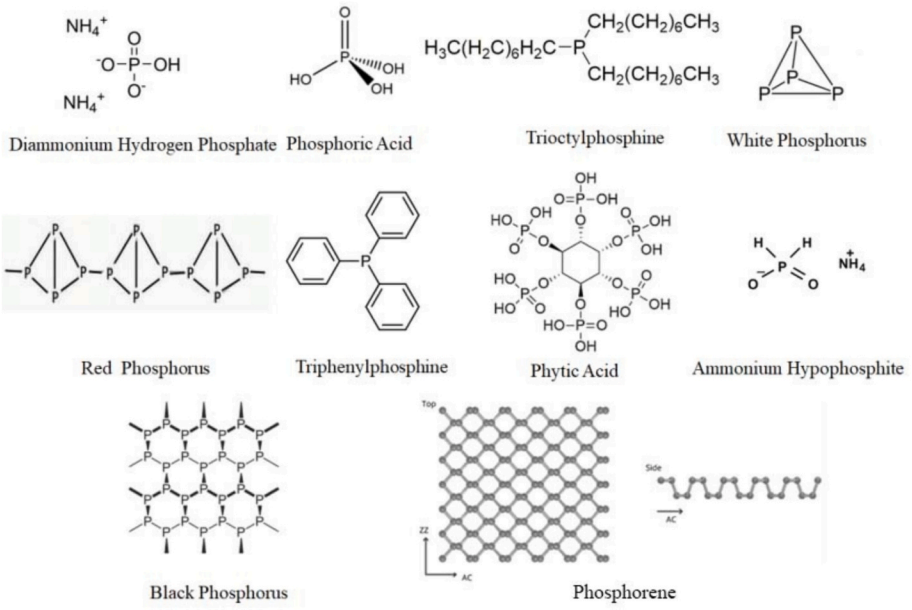

Fig. 3. Structures of different kinds of phosphorus sources.

ruthenium (Ru), rhodium (Rh), etc. are commonly employed as the co-catalyst to achieve the electron trap strategy [12–15]. The limited availability and high cost of precious metals present constraints on their widespread applications, necessitating the exploration of advanced active catalysts composed of economically viable earth-abundant materials. Nowadays, non-noble metal-based materials, such as metals (Mo, Co, Ni, etc.) [16–18], metal oxides (Cu_2O, MgO, etc.) [19,20], metal chalcogenides (MoS_2, CoSe, NiS, VS_4, etc.) [20–23], metal nitrides (Mo_2N, Ni_3N, W_2N, Co_2N, etc.) [24–26], metal carbides (Mo_2C, Ti_3C_2 MXene, WC, Co_3C, etc.) [27–30], and transition metal phosphides (Ni_2P, Ni_4P_5, FeP, CoP, etc.) [31–34] have been studied as alternative co-catalysts for photocatalytic H_2 production. Among them, transition-metal phosphides (TMPs) have attracted considerable attention owing to their unique physicochemical properties, including excellent heat and electrical conductivity, good thermal and chemical stability, relatively small band gap value, etc. Significant achievements have been achieved in recent years regarding the development of co-catalysts for photocatalytic H_2 production utilizing TMPs [35–37]. It is imperative to summarize these advancements and promote further progress in this field, thereby advancing the state-of-the-art design of TMPs-based photocatalysts for H_2 production.

Herein, this review provides a comprehensive summary of the recent significant advancements in TMPs as co-catalysts for highly efficient and durable photocatalytic hydrogen evolution reaction (HER). Firstly, a concise overview of the typical characteristics exhibited by TMPs is introduced. Subsequently, the synthesis strategies of numerous TMPs derived from various phosphorus sources are comprehensively summarized. Furthermore, recent research efforts focused on exploring the application of TMPs as photocatalytic co-catalysts in H_2 generation reactions are discussed. Finally, the current bottlenecks, challenges, and future research directions aiming at augmenting the performance of TMPs are elucidated.

2. Brief historical review and structure of TMPs

The emergence of TMPs as a highly promising (co)catalyst material in diverse catalytic domains can be attributed to their exceptional efficiency and consistent activity. It is worth noting that the history of synthetic TMP can be traced back to the 18th century [38]. However, in nearly two hundred years, people have not found a suitable application for TMPs. Until the 1950s, TMPs were gradually used in metallurgy, pesticides, hydrodesulfurization, hydrodenitrification, hydrodeoxygenation (HDO), and other fields [39]. In the 1990s, researchers found that the deposition of phosphorus and metal on the electrode in the form of an amorphous alloy exhibited a good electrolytic activity of HER from water. Typically, amorphous materials, which are generally obtained at low temperature, offer the advantages such as a large surface area and high catalytic activity. However, these materials usually suffer from low crystallinity, resulting in poor stability. In 2005, the high electrolytic HER activity of Ni_2P (001) was predicted by Liu et al. through a theoretical analysis. Until 2013, Zhang's group utilized the ion exchange method to synthesize porous FeP nanosheets and demonstrated for the first time in the world, that nano-transition metal phosphating serves as an efficient catalyst for HER [40]. In the same year, Schaak's research group experimentally confirmed the high electrolytic HER activity of Ni_2P [41]. Later, the research group led by Sun successfully fabricated a series of self-supporting TMP nanoarrays exhibiting exceptional electrolysis HER performance [42–46]. From this point on, the investigation and application of TMPs have been extensively explored in various fields related to energy storage and conversion.

In principle, TMPs can be utilized as P-doped metallic alloys. Based on the data shown in Fig. 2a, it is evident that a vast majority of transition metal elements exhibit reactivity toward phosphorus, resulting in the formation of respective TMPs. The typical structures of some common TMPs are illustrated in Fig. 2b [47]. Due to the electronegativity of P being slightly greater than that of metal, P in phosphide is slightly negatively charged, while metal is slightly positively charged [48]. In other words, not only can the negatively charged P play a role in attracting protons, but this covalent metal-phosphorus bond can also increase the stability of the TMPs. Besides, the density functional theory (DFT) simulation indicates that the involvement of P atoms is pivotal in various catalytic reactions [49]. Moreover, based on the inorganic crystal structure database, P can form a large family of TMPs with different stoichiometric ratios (P-poor to P-rich TMPs) and diverse crystal structures. The corresponding composition/structure properties can be coordinated by changing the P amount. For instance, there are more than nine stoichiometric variations of nickel phosphides with diverse Ni: P ratios [50]. Some of them are presented in Fig. 2c. Moreover, it is reported that P-poor (metal rich) TMPs have high conductivity [51,52]. In sharp contrast, partial P-rich TMPs show semiconductor properties due to the significant electron delocalization restriction

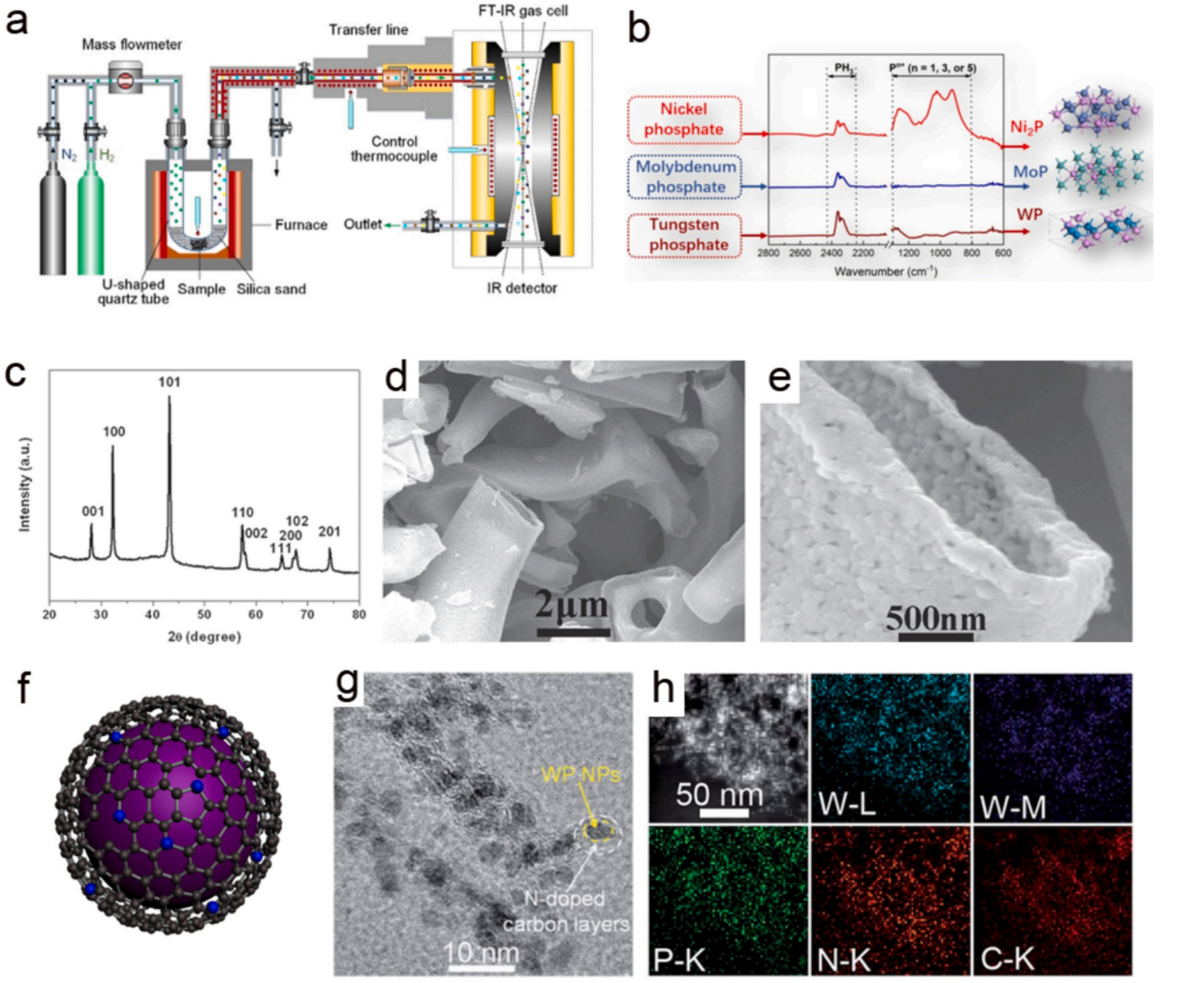

Fig. 4. (a) The TPR-IR) apparatus. (b) Schematic illustration of H_2 reducing metal phosphates. Reproduced with permission from ref. 58. (c) XRD pattern of MoP. (d) Low- and (e) high–magnification SEM images of MoP. Reprinted with permission from ref. 59. (f) Schematic for WP NPs@NC, (g and h) TEM and STEM mapping images of WP NPs@NC. Reprinted with permission from ref. 60.

imposed by P atoms on the metal [53,54]. To enhance the conductivity of P-rich TMPs, our previous studies have demonstrated that the poor conductivity of these materials can be effectively modulated through encapsulation with heteroatom (such as N, P, etc.)-doped carbon [46,55–57]. In other words, TMPs possess a variety of unique physicochemical properties, including excellent heat and electrical conductivity, good thermal and chemical stability, relatively small band gap value, etc.

3. Synthesis strategies of TMPs

Numerous strategies are available for the preparation of TMPs. In this section, we classify the synthesis methods based on distinct phosphorus sources, including phosphate, organophosphorus, phytic acid (PA), hypophosphite (NaH_2PO_2 or $NH_4H_2PO_2$), red/black phosphorus, and so on. Specifically, Fig. 3 illustrates the molecular structure of a partial phosphorous compound.

3.1. Direct reduction from metal phosphate for the TMPs fabrication

The reduction of metal phosphates at elevated temperatures in a reductive atmosphere, such as H_2, represents a promising approach for the fabrication of TMPs (Eq. (5)). By employing a temperature-programmed reduction-infrared spectroscopy (TPR-IR) apparatus (Fig. 4a), Sheng et al. demonstrated that during the reduction process of Ni, Mo, and W phosphate precursors to their respective phosphides, gaseous PH_3 and P^{n+} species were detected at temperature ~ 200 °C (Fig. 4b) [58]. For instance, as shown in Figs. 4c-e, MoP with macro-size and irregular morphologies can be synthesized by using $NH_4H_2PO_4$, $(NH_4)_2HPO_4$, etc. as the phosphorus sources under the H_2 atmosphere. There are two shortages of this approach: i) It needs dangerous gas (H_2) as a reductant at high temperatures; ii) The product is always macro-sized with irregular morphologies [59]. To circumvent the utilization of the dangerous H_2 at high temperatures, as shown in Figs. 4f-h, our previous studies have demonstrated a facile one-step method for synthesizing N-doped carbon encapsulating tungsten phosphide nanoparticles (WP NPs@NC), employing melamine as the reductant under 800 °C [60]. Subsequently, a wide range of TMPs, including CoP, Co_2P, FeP, Fe_2P, Ni_2P, $Ni_{12}P_5$, WP, MoP, $Ru_xCo_{1-x}P$, etc., embedded within a heteroatom(N, P, etc.)-doped carbon materials were reported by our research group as well as others researchers by using the similar methodologies [61–64]. More importantly, the unique nanostructure of TMPs

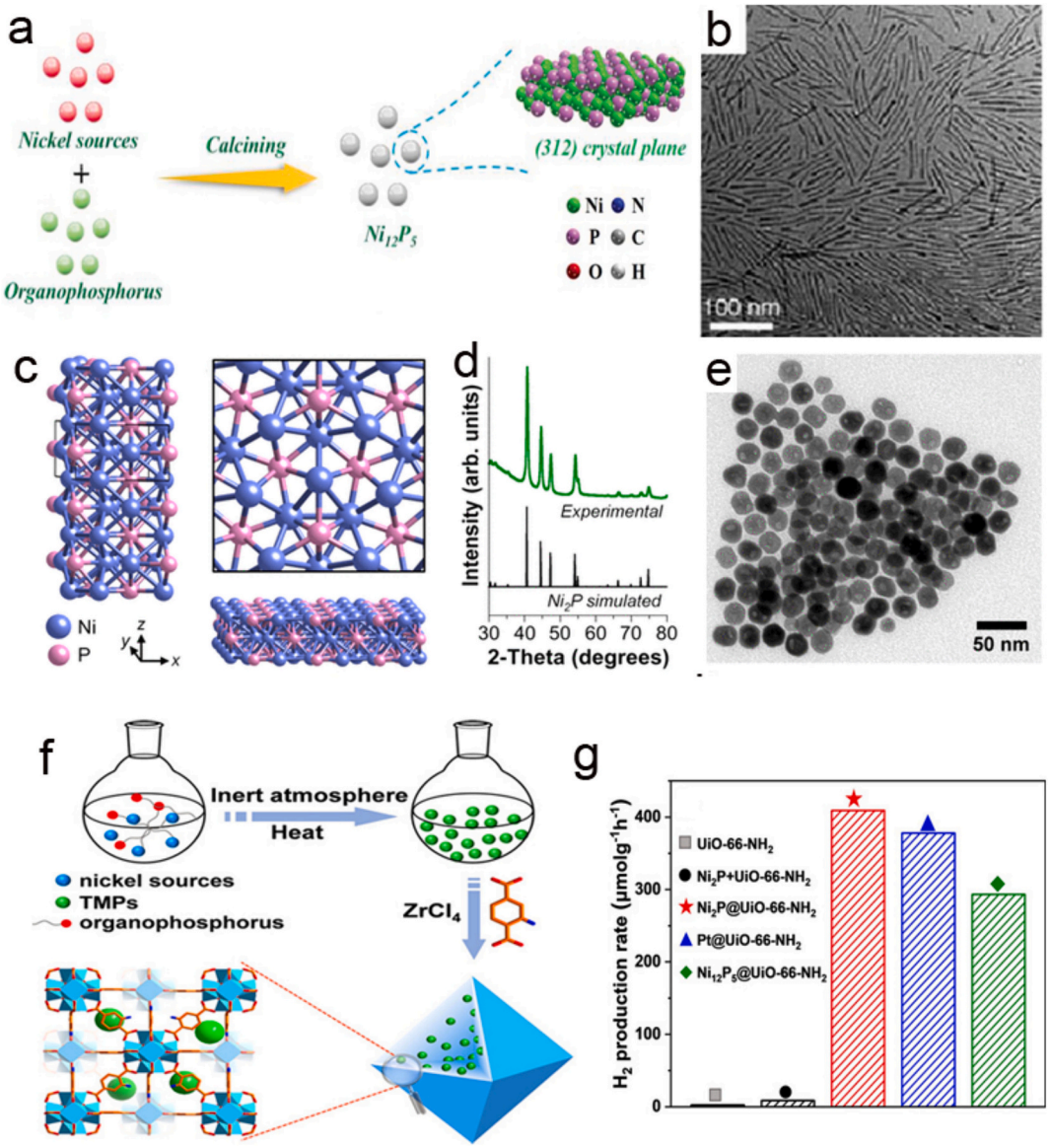

Fig. 5. (a) Schematic of the synthetic process for the $Ni_{12}P_5$. Reproduced with permission from ref. 33. (b) TEM image of FeP nanorods. Reproduced with permission from ref. 65. (c) Crystal structure of Ni_2P nanoparticles. (d) XRD pattern, (e) TEM image of Ni_2P nanoparticles. Reprinted with permission from ref. 41. (f) Schematic illustration for the synthesis of TMPs and TMPs@UiO-66-NH_2. (g) The photocatalytic hydrogen production rates of different materials. Reproduced with permission from ref. 67.

embedded within heteroatom-doped not only avoids aggregation, but also guarantees robust cyclic stability of the electrocatalyst during the catalytic reaction process.

$$M_x(PO_4)_y + H_2 \rightarrow M_xP_y + H_2O \quad (5)$$

3.2. Uniform TMPs synthesis from thermal decomposition of organophosphorus

Triphenylphosphine (TPP), trioctylphosphine (TOP), and trioctylphosphine oxide (TOPO) are commonly employed as the phosphorous source for the synthesis of TMPs in an organic solvent, owing to their ability to undergo C—P bond cleavage at a higher temperature. Consequently, metal precursors such as metal carbonyl compounds and metal acetylacetonates can undergo phosphorization in the presence of TOP/TPP/TOPO. The typical schematic of the synthetic process for the $Ni_{12}P_5$ is shown in Fig. 5a [33]. Similarly, a series of ultrasmall structure, uniform-size noble and non-noble TMPs, including FeP nanorods (Fig. 5b), Ni_2P nanoparticles (Figs. 5c-e), CoP, MoP, WP, Rh_2P nanosheets, etc. can be synthesized using organophosphorus as the P resource [41,65,66]. It is worth noting that Jiang's group demonstrate the successful incorporation of Ni_2P or $Ni_{12}P_5$ into a representative MOF (UiO-66-NH_2), resulting in excellent photocatalytic H_2 activity (Figs. 5f and g) [67]. In general, the utilization of organophosphorus as a phosphorus source offers inherent advantages in yielding products with consistently uniform morphologies, ultrasmall dimensions, and large surface areas. This synthesis method is challenged by the high-temperature decomposition of organic reagents due to their corrosive and flammable nature. The catalytic activity of TMPs may be further influenced by the organic ligand that inevitably adsorbs onto the surface of nanomaterials.

3.3. Versatile formation of TMPs with hypophosphite or PH_3

The utilization of hypophosphite ($NH_4H_2PO_2$/NaH_2PO_2) as the phosphorus source represents an additional efficient and readily accessible approach for the synthesis of TMPs. The synthesis scheme can be

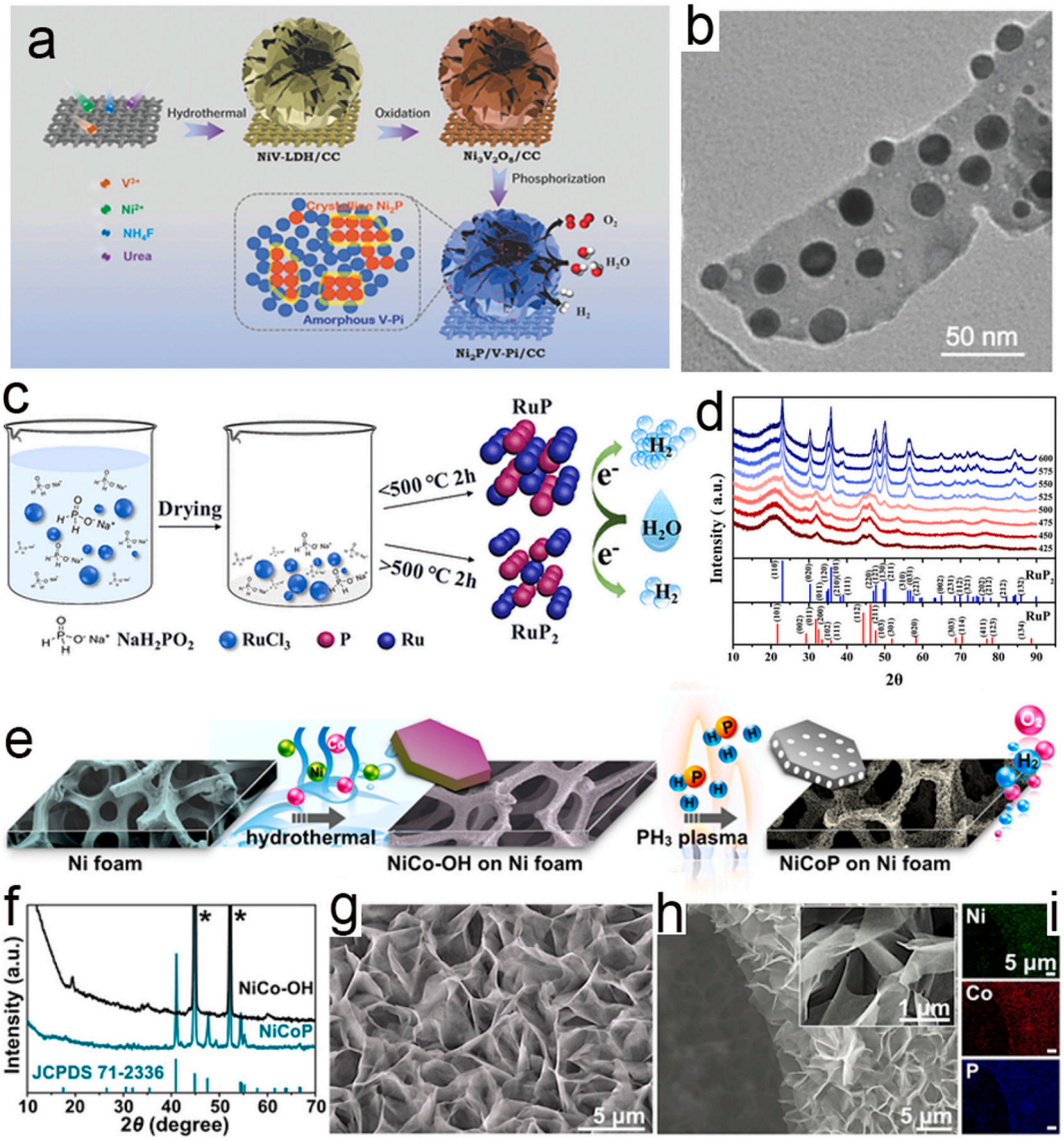

Fig. 6. (a) The synthetic procedure of Ni_2P/V-Pi/CC. (b) TEM image for Ni_2P/V-Pi. Reproduced with permission from ref. 85. (c) The synthesis procedure of RuP_x for HER. (d) XRD patterns of RuP_x synthesized in different temperatures. Reproduced with permission from ref. 86. (e) Synthetic route of the NiCoP nanostructure. (f) XRD patterns of NiCo-OH and NiCoP. SEM images of (g) NiCo-OH and (h) NiCoP. (i) EDS elemental maps of the NiCoP. Reproduced with permission from ref. 87.

delineated as follows: Initially, the TM precursor (such as metal or metal oxides/hydroxides/sulfides/salts) and hypophosphite are directly placed in porcelain boats. Subsequently, by heating the hypophosphite to liberate PH_3 as the P source, the TM precursor undergoes a reaction with the PH_3 gas to yield TMPs [68]. Using this method, it is reported that almost all metal (Fe, Co, Ni, Cu, Mo, W, Ru, Pt, Ir, etc.) based TMPs can be obtained [46,69–84]. For example, recently, the research team led by Han presented a novel flower-like nanohybrid architecture comprising Ni_2P nanocrystals anchored on amorphous V-phosphates nanosheets (Figs. 6a and b) [85]. Additionally, precise control of phosphorization conditions, including temperature, hypophosphite content, and the presence of phosphorus-rich (P-rich) or phosphorus-deficient (P-deficient) TMPs can be employed to obtain desired outcomes. For instance, the synthesis of pure RuP and RuP_2 was successfully demonstrated by Chang et al. through precise temperature control during the phosphorization process (Figs. 6c and d) [86]. Additionally, as depicted in the schematic shown in Fig. 6e, Alshareef and colleagues have successfully synthesized bimetallic metal phosphides of NiCoP nanosheets (Figs. 6f-i) through a novel PH_3 plasma-assisted method, involving the phosphorization of the NiCo–OH precursor [87]. Although this method is applicable for the preparation of various TMPs, the typical drawback is the generation of toxic and self-igniting PH_3 products during the synthesis process [55].

3.4. Clean TMPs fabrication from PA

PA, a naturally occurring compound with six phosphonic acid groups, exhibits environmental friendliness and non-toxicity, and serves as both an effective source of P as well as a facilitator for rapid linking of metal ions. Our group initially found a facile and simple way for the synthesis of a series of non-noble/noble (CoP, FeP, Ni_2P, MoP, Rh_2P, etc.) or P-rich/deficient (RuP_2/Ru_2P, FeP/Fe_2P, etc.) TMPs embedded within heteroatom-doped carbon matrix using melamine and PA as the reductant and P source [55,57,61,88–92], respectively. For example, as illustrated in Fig. 7a, the RuP_2 nanoparticles encapsulated within an N, P co-doped carbon (RuP_2@NPC) can be obtained using PA as the P source [57]. Additionally, Wang and Lou's group developed a facile way for synthesizing the CoP/C nanoboxes and Ni-doped FeP/C hollow nanorods by pyrolyzing PA-etched ZIF-67 (Fig. 7b) [93], and Ni-doped MIL-88 A (Fig. 7c), respectively [94]. The compound PA is inherently

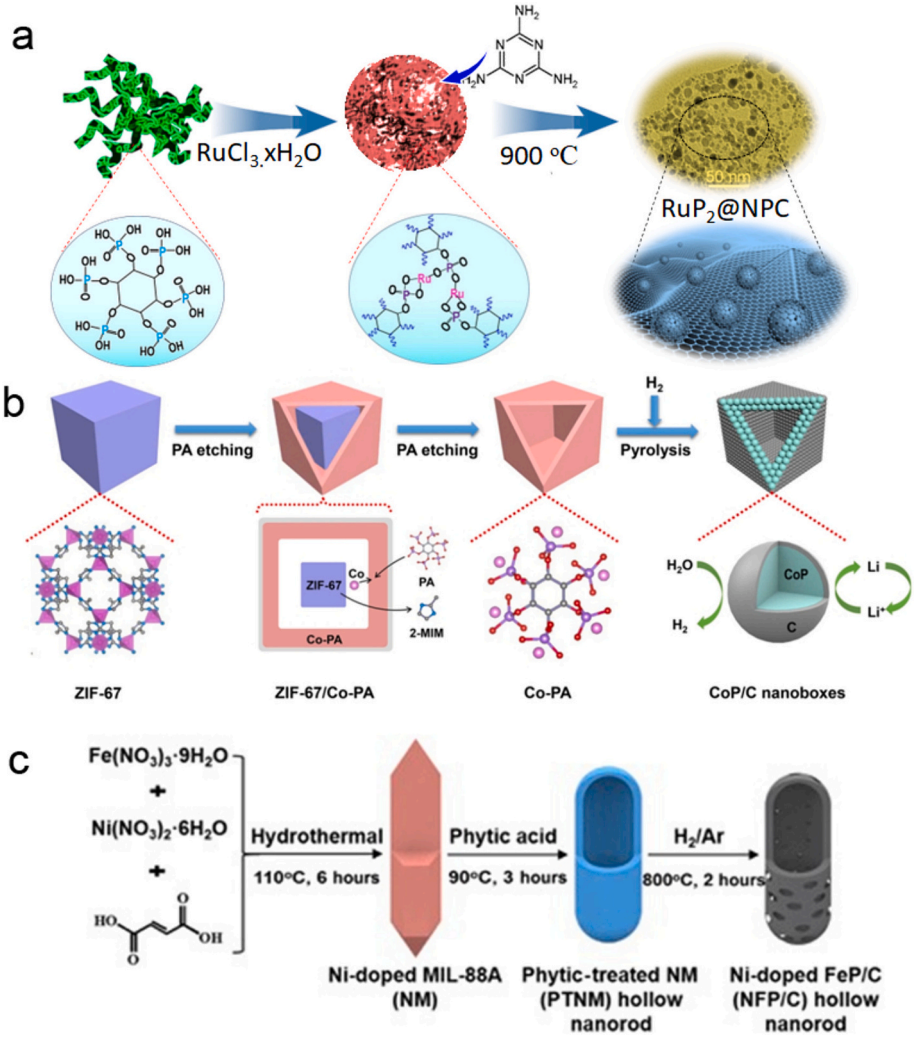

Fig. 7. (a) Schematic representation for the synthesis of RuP_2@NPC material. Reproduced with permission from ref. 54. (b) The formation procedure of the CoP/C nanoboxes. Reprinted with permission from ref. 86. (c) Schematic representation depicting the synthesis of Ni-doped FeP/C. Reprinted with permission from ref. 87.

environmentally friendly and renewable, aligning with the principles of sustainability. Additionally, under temperature-programmed reduction conditions, the P—O bond undergoes cleavage, releasing P as a source of phosphorus for the formation of metal phosphides. Therefore, it is reasonable to say that PA is an eco-friendly P source when employed in the preparation of TMPs.

3.5. *General TMPs synthetic strategies from red/black/yellow phosphorus*

The employment of solvothermal, hydrothermal, or high-temperature pyrolysis techniques, utilizing metal precursor and red/black/yellow phosphorus as reactants, represents a general strategy for the preparation of TMPs. It is noteworthy that based on the black phosphorene (BP) being a typical 2D semiconductor, a series TMPs/BP heterostructure photocatalyst/co-catalyst system has been reported by different groups [95–99]. For example, Co_2P/BP heterostructure photocatalyst is designed and synthesized by Yuan et al. (Fig. 8a). More importantly, as illustrated in Fig. 8b, the photocatalytic H_2 generation rate of the Co_2P/BP nanosheets photocatalyst exhibits a 39.7-fold enhancement compared to that of bare BP nanosheets [95]. It is reported that P-rich TMPs always can be synthesized by using red phosphorous as the P precursor. For instance, Wu et al. reported that CoP_3 nanoplate arrays could be obtained by a facile topotactic phosphidation method under hydrothermal conditions (Figs. 8d-f) [100]. Mu's group reported the successful fabrication of a P-rich bimetallic diphosphide pair (FeP_2–NiP_2) using red phosphorus as the reaction precursor (Figs. 8g and h) [56]. Nevertheless, it should be highlighted that red phosphorus generates white phosphorus vapor at elevated temperatures, which is highly flammable. This process is inherently unsafe due to the inherently hazardous nature of the reaction. Moreover, Bao et al. demonstrated the formation of a binding heterojunction, denoted as BP/NiP_3, utilizing black phosphorus as the precursor to produce BP nanosheets and P-rich TMPs [101]. Du and colleagues have employed yellow phosphorus as a starting material for the synthesis of Ni_2P at temperatures below 120 °C [102].

3.6. *TMPs formation from other P sources*

Pyrolyzing the compounds containing the metal precursor and P source is also an effective method to prepare TMPs. For instance, Schipper et al. have demonstrated the synthesis of phase-pure thin films of Fe_2P, FeP and Fe_3P from $Fe(CO)_4PH_3$ (1), $Fe(CO)_4PtBuH_2$ (2) or $Fe(CO)_4P(H)tBu_2$ (3) and $H_2Fe_3(CO)_9PtBu$ (4) precursors (Figs. 9a and b) [103]. The carbon-encapsulated TMP materials were obtained by Weng et al. through pyrolysis of N-, S-, and P-containing MOFs [104]. Some of the TMPs, such as iron phosphide film [105], amorphous cobalt-nickel-phosphide [106], and rhodium phosphide [107] can be prepared by electrodeposition. More recently, Zhou's group demonstrated the

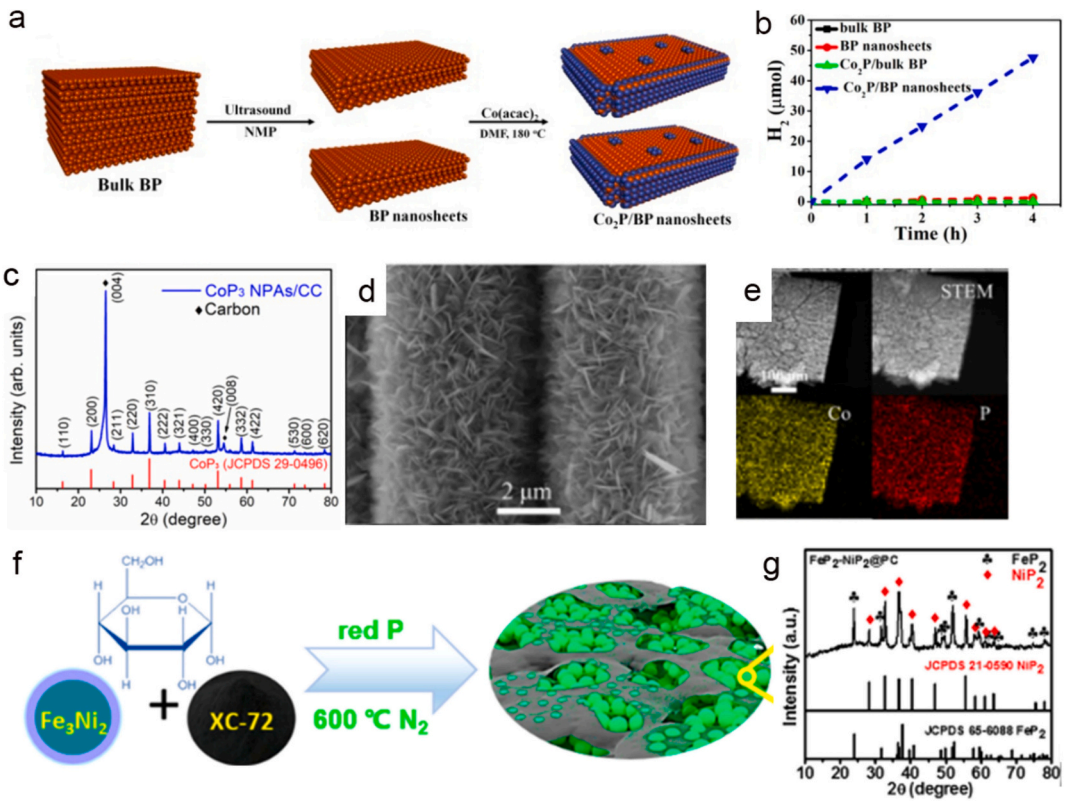

Fig. 8. (a) Schematic representation of the synthesis process for Co_2P/BP material. (b) Temporal evolution of hydrogen over various photocatalysts. Reproduced with permission from ref. 95. (c) XRD pattern, (d) SEM, and (e) STEM images of CoP_3 nanoplate arrays. Reproduced with permission from ref. 100. (f) The schematic diagram for the fabrication of FeP_2-NiP_2@PC. (g) XRD pattern of FeP_2-NiP_2@PC. Reproduced with permission from ref. 56.

fabrication of several TMPs, including CrP, Co_2P, Ru_2P, and Ni_3P, through a solid–solid reaction using microorganisms as the phosphorus source [108–112]. Figs. 9c-e depict the typical synthesis process, crystal structure, and morphology of Co_2P. In addition, the research conducted by Feng's group reveals that a range of 2D TMPs, such as $Ni_{12}P_5$, Co_2P, and $Co_xFe_{2-x}P$, can be synthesized utilizing phosphorene sheets as the source of phosphorus and employing 2D templates (Figs. 9f-j) [113]. In general, reactants possessing both P and metal elementals can serve as the precursors for the synthesis of TMPs.

4. Recent advancements of TMPs in photocatalytic H_2 production

In recent years, TMPs have attracted significant attention in energy storage and conversion fields. Harnessing the intrinsic semiconductor or metallic properties, TMPs have also been applied as photocatalysts and cocatalysts for a wide range of photocatalytic redox reactions. Among the extensively studied TMPs, Ni/Fe/Co/Cu/Mo/W-based phosphides have been widely employed as co-catalysts for photocatalytic hydrogen generation. In the subsequent section, a detailed introduction and discussion of the performances and mechanisms exhibited by these TMPs in photocatalytic hydrogen generation are presented.

4.1. Iron group TMPs as co-catalysts for photocatalytic H_2 production under visible light

The development and investigation of non-precious metal co-catalysts hold significant importance in achieving efficient photocatalytic hydrogen production. Iron group elementals (Fe, Co, Ni) are earth-abundant and low-cost transition metals. Therefore, iron group-based materials are widely used as catalysts for many kinds of catalytic reactions. Fe/Co/Ni-based sulfides, selenides, phosphides, etc. are widely used as HER electrocatalysts with high performance [114–117]. More recently, iron group TMPs have emerged as promising alternatives to precious-metal co-catalysts for efficient photocatalytic hydrogen generation. For example, the photocatalytic activity of sulfur-doped g-C_3N_4 (S-CN) decorated with M_2P (M = Fe, Co, Ni) as a cocatalyst was investigated for visible light-induced H_2 generation by Sun et al. (Figs. 10a and c). As shown in Fig. 10b, the optimum co-catalyst of Ni_2P is approximately 22.7 times higher than that of the pristine S-CN under identical conditions [118]. Similarly, Ma et al. reported the M_2P (M = Fe, Co, Ni) combined with $CdIn_2S_4$ to achieve robust photocatalytic activity. For example, the $Fe_2P/CdIn_2S_4$, $Co_2P/CdIn_2S_4$, and $Ni_2P/CdIn_2S_4$ catalysts exhibited maximum H_2 production rate at 316.8, 471.9 and 810.0 μmol h^{-1} g^{-1}, respectively, which were 2.4-fold, 3.6-fold and 6.2-fold higher than that of $CdIn_2S_4$-Pt (130.5 μmol g^{-1} h^{-1}) [119]. Du's group demonstrated that the integration of CoP_x, Ni_2P, FeP, and NiCoP with CdS as semiconductors exhibits remarkable activity in photocatalytic H_2 generation under visible light [102,120–122]. The Ni_2P/CdS nanorods system, as an example, exhibits remarkably high catalytic activity and exceptional durability (> 90 h). Under optimal conditions, the maximum observed rate of H_2 generation reached approximately 1200 mmol h^{-1} mg^{-1} (Figs. 10d-g) [102]. Moreover, it is reported that FeP nanoparticles immobilized on TiO_2 can photocatalytically produce H_2 in both acidic and neutral media under ultraviolet illumination [123]. The potential of red phosphorus as a visible-light-driven semiconductor for photocatalytic hydrogen production has been acknowledged. Nevertheless, its performance is constrained by the sluggish surface reaction kinetics and rapid recombination of charge carriers. To tackle this issue, Yang et al. developed an in situ phosphorization strategy to prepare CoP_2-modified red phosphorus heterostructure (Figs. 10h and i). By optimizing the CoP_2 content in the heterostructure, the hybrid system achieves a remarkable hydrogen evolution rate of 11.79 μmol h^{-1} under visible light irradiation,

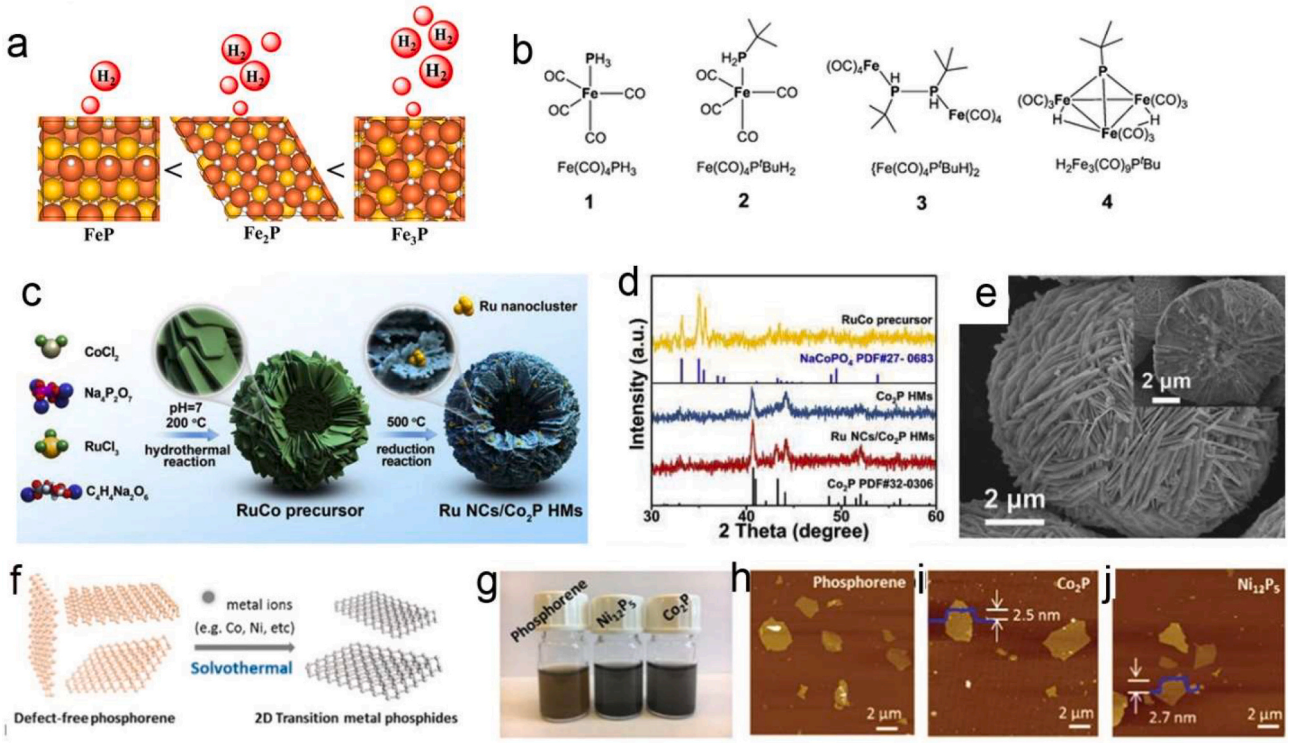

Fig. 9. (a) Sing-source precursor-derived iron phosphides. (b) Molecular structure of $Fe(CO)_4PH_3$ (1), $Fe(CO)_4PtBuH_2$ (2) or $Fe(CO)_4P(H)tBu_2$ (3) and $H_2Fe_3(CO)_9PtBu$ (4). Reproduced with permission from ref. 103. (c) Schematic representation of the synthetic procedure for Ru NCs/Co_2P hollow microspheres. (d) XRD pattern of RuCo precursor, Ru NCs/Co_2P hollow microspheres and Co_2P hollow microspheres. (e) Typical SEM images of RuCo precursor. Reprinted with permission from ref. 110. (f) Transformation of phosphorene to 2D TMPs. (g) Optical photos of phosphorene, $Ni_{12}P_5$. and Co_2P dispersions in DMF. (h–j) Atomic force microscopy images of phosphorene, Co_2P, and $Ni_{12}P_5$, respective. Reprinted with permission from ref. 113.

surpassing that of red phosphorus with Pt as a co-catalyst by a factor of 3.5 [124].

4.2. *Copper phosphides for p-n junction formation to boost the charge separation*

Copper phosphide (Cu_3P), as a p-type semiconductor, has been demonstrated as an effective co-catalyst for various photocatalytic reactions such as H_2 production, CO_2 reduction, and antibiotic degradation when supported by semiconductors like CdS, TiO_2, ZnS, C_3N_4, BiOCl, $BiVO_4$, etc. [125–130]. As a typical example, in 2015, the study by Sun et al. represents the pioneering discovery that p-type Cu_3P can function as an effective material for enhancing the photocatalytic H_2 production from H_2O when combined with n-type CdS nanorods (Fig. 11a). Attributed to the presence of p–n junction, the Cu_3P/CdS nanorods exhibit rapid charge transfer, enhancing photocatalytic H_2 evolution performance (~200 mmol h^{-1} mg^{-1}) under visible light irradiation (Figs. 11b and c). Moreover, as illustrated in Figs. 11d-f, the research conducted by Liu's group demonstrated the outstanding photocatalytic H_2 production performance of g-C_3N_4 loaded with both Cu_3P and $Cu_{97}P_3$. Specifically, the photocatalytic H_2 production rate is 343 μmol h^{-1} g^{-1} and 162.9 μmol h^{-1} g^{-1} for Cu_3P/g-C_3N_4 and $Cu_{97}P_3$/g-C_3N_4, respectively [131]. Recently, Sun's group reported the synthesis of a p-type Cu_3P/n-type g-C_3N_4 heterojunction by phosphorization of a $CuCl(OH)_3$/gC_3N_4 precursor (Fig. 11g). In this system, the Cu_3P material exhibited dual functionalities, namely promoting the efficient separation of charge carriers and reducing the overpotential for H_2 evolution. Additionally, they further demonstrated that Cu_3P nanoparticles accumulated electrons while g-C_3N_4 nanosheet enriched holes, indicating a *Z*-scheme carrier transfer pathway (Fig. 11i) [132]. As a result, the p-type Cu_3P/n-type g-C_3N_4 heterojunction achieves a maximum catalytic activity of 808 μmol h^{-1} g^{-1}(Fig. 11h).

4.3. *Molybdenum/tungsten phosphides for efficient "H delivery" and charge transfer*

Traditionally, molybdenum-based materials show high electro (photo)catalytic activity for HER [133–139]. Especially, the MoP catalyst demonstrates a highly efficient 'H delivery' system, exhibiting minimal H binding at specific H coverage [140]. The metallic nature of MoP facilitates electron attraction and effectively enhances the migration of photo-induced charges [54]. Therefore, the utilization of MoP as an exceptionally efficient co-catalyst for photocatalytic hydrogen production has garnered increasing attention [141–143]. Du's group initially reported MoP as an exceptionally efficient cocatalyst for visible light-photocatalytic H_2 production. By employing MoP/CdS as the metal-semiconductor system (Fig. 12a), a significant enhancement in photocatalytic H_2 generation performance under visible light was observed. Specifically, the optimized MoP/CdS exhibits an H_2 generation rate of 163.2 mmol h^{-1} g^{-1}, surpassing that of bare CdS by over 20-fold (Fig. 12b). This remarkable improvement can be ascribed to the fast charge transfer at the MoP and CdS interface, facilitated by suitable Fermi level alignment (Fig. 12c) [144]. Additionally, MoP was synthesized by Cheng et al. through an innovative and simplified phosphorization process conducted under ambient air conditions and low temperatures. Cheng et al. synthesized MoP by a novel and simplified phosphorization process at a relatively low temperature under an ambient-air atmosphere [145]. The MoP/g-C_3N_4 hybrids exhibit excellent performance in photocatalytic H_2-production performance following their coupling, with the co-catalytic effect of MoP and corresponding synergistic interaction between MoP and g-C_3N_4 being systematically investigated. The formation of metal-N bond in MoP/g-C_3N_4 was considered to be a crucial factor contributing to the favorable photocatalytic activity (Figs. 12d and e).

Based on the similarity between tungsten and molybdenum (same

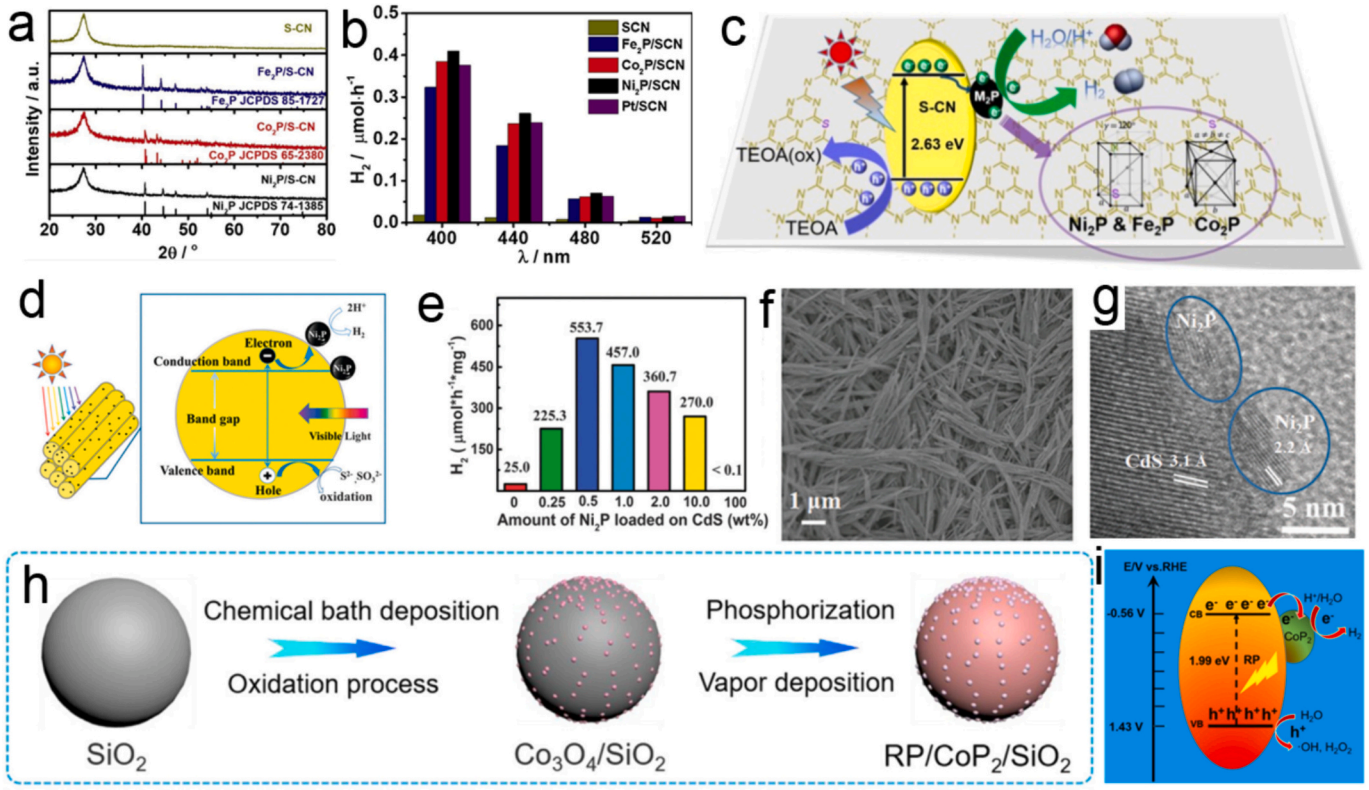

Fig. 10. (a) XRD patterns and (b) photocatalytic H_2–production rates of S-CN, Fe_2P/S-CN, Co_2P/S-CN, Ni_2P/S-CN. (c) Schematic representation of the photocatalytic H_2-production of M_2P/S-CN. Reproduced with permission from ref. 118. (d) Schematic depiction of photocatalytic H_2 production from H_2O with CdS/NRs-Ni_2P photocatalyst system. (e) The H_2 evolution rate for Ni_2P/CdS NR photocatalysts loaded with varying amounts of Ni_2P (f and g) SEM and HRTEM images of Ni_2P/CdS NRs. Reproduced with permission from ref. 102. (h) Schematic representation of synthetic procedure of RP/CoP_2/SiO_2. (i) Mechanism representation for the photocatalytic H_2-production using RP/CoP_2(x)/SiO_2. Reproduced with permission from ref. 124.

group on the periodic table of elements), tungsten phosphide also has been developed as a co-catalyst for photocatalytic H_2 production recently [146–150]. For example, Zhang et al. employed the conventional temperature programming reduction method to synthesize WP nanoparticles, which were subsequently immobilized onto the surface of CdS (Fig. 12f). After incorporating 4.0 wt% WP, the hybrids of CdS/WP demonstrate an H_2-production rate of 155.2 μmol h^{-1}, representing an increase by a factor of 11.67 compared to that of CdS (Figs. 12g and h) [150].

4.4. Other metal or bi-metallic phosphides

In addition to the development of monometallic phosphides based on Ni, Fe, Cu, Co, Mo, and W as co-catalysts for photocatalytic H_2 evolution, recent investigations have also been conducted on other metal or bimetallic, and even multi-metallic phosphides supported on semiconductors for H_2 generation through photocatalysis. For instance, a series of noble-metal-based phosphides have been reported by different research groups as a co-catalyst for photocatalytic H_2-production, including amorphous ruthenium phosphide quantum dots, Ru_xP nanoparticles, ruthenium doped rhenium phosphide, Rh_xP nano-species, Rh-phosphide, platinum diphosphide nanodots, etc. [151–156] As a typical example, Yu's group indicated the uniform distribution of ultrafine PtP_2 nanodots on a carbon layer (C), which were subsequently integrated with CdS to fabricate the PtP_2@C/CdS (Figs. 13a and b). The PtP_2@C/CdS material shows an H_2 generation rate of 9.76 mmol h^{-1} g^{-1} with an apparent quantum yield of 41.67% (~420 nm) under visible-light irradiation, surpassing the blank CdS and Pt@C/CdS by factors of 34.8 and 2.2 (Fig. 13c), respectively. Moreover, it is suggested that bi/tri-metallic phosphides gain significant attention in the field of HER owing to their much lower overpotential, enhanced conductivity, and diminished charge carrier transfer impedance compared to those of single metal phosphides. In other words, the bi/tri-metallic phosphides exhibit greater potential as non-noble promoters for photocatalytic H_2 generation from water splitting, in contrast to mono-metallic phosphides. Relevant investigations and studies on such topics have been extensively conducted in recent years [157–160]. For instance, the utilization of bimetallic phosphide NiCoP as a modifier for g-C_3N_4 has been reported to exhibit a significantly enhanced H_2 evolution rate compared to Co_2P/g-C_3N_4 and Ni_2P/g-C_3N_4. This enhancement is primarily ascribed to the synergistic effect resulting from the Schottky barrier and the lower overpotential compared to that of Ni_2P or Co_2P counterparts (Figs. 13d and e) [157]. In addition to NiCoP as an ideal cocatalyst, NiFeP, MnCoP, Cu_3P-Ni_2P, etc. also exhibit the desired photocatalytic H_2 generation activity under simulated solar light irradiation [36,158].

In recent years, the utilization of TMPs as co-catalysts in photocatalytic H_2 production has exhibited significant advancements in terms of enhanced production efficiency, positioning it as a promising alternative within the realm of semiconductor photocatalysts. The photocatalytic H_2-production activities of the TMPs/semiconductor system are presented in Table 1. However, further extensive research is imperative to enhance its viability for commercial applications.

4.5. TMPs directly as the host photocatalysts for H_2 production

It is noteworthy that in photocatalytic reactions, the majority of TMPs, acting as co-catalysts, provide a significant number of active species and accept photoinduced electrons from semiconductor catalysts. Nevertheless, some TMPs can also function as host materials. For example, Chen's research group has reported the discovery of semi-metallic MoP_2 nanoparticles, which exhibit promising potential as a novel photocatalyst for efficient H_2 production from H_2O under visible

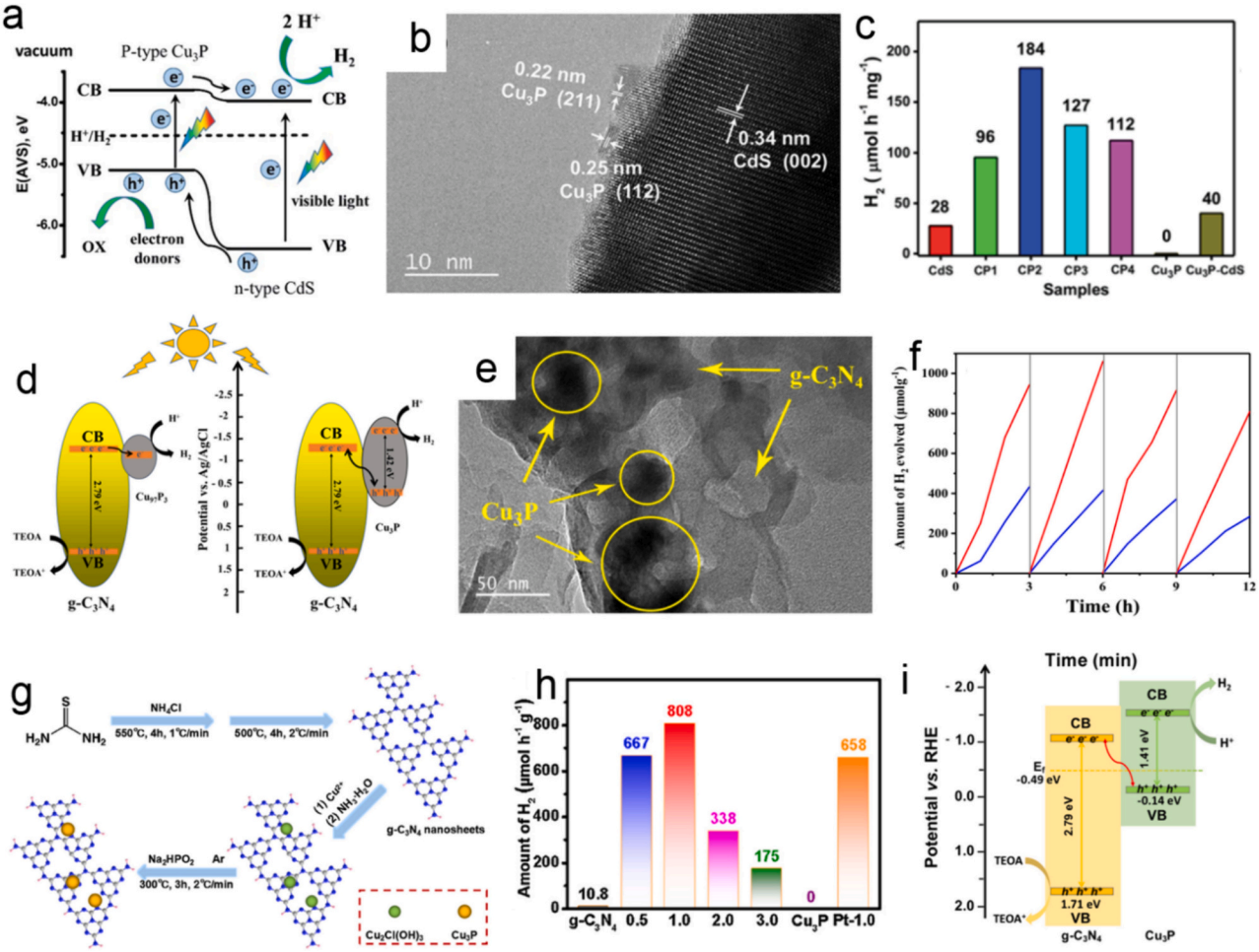

Fig. 11. (a) Mechanism illustrating photocatalytic H_2-production by the Cu_3P/CdS compound. (b) HRTEM image of the CP2 sample. (c) Comparison of photocatalytic H_2-production rates of CdS with control samples. Reproduced with permission from ref. 125. (d) Schematic illustration of the charge separation and transfer mechanism on g-C_3N_4 catalysts decorated with copper phosphide (Cu_3P, $Cu_{97}P_3$). (e) TEM images of CN–Cu_3P-1. (f) Stability curves for CN-Cu_3P-1 (red) and CN-$Cu_{97}P_3$–1 (blue). Reprinted with permission from ref. 131. (g) Synthesis pathway of Cu_3P/g-C_3N_4 compound material. (h) H_2-production rate of g-C_3N_4, Cu_3P, Cu_3P/g-C_3N_4 and Pt/g-C_3N_4–1.0. (i) The potential charge transfer mechanism for H_2-evolution for Cu_3P/g-C_3N_4. Reproduced with permission from ref. 132. (For interpretation of the references to colour in this figure legend, the reader is referred to the web version of this article.)

light irradiation (Figs. 14a-d) [161]. Similarly, the semimetallic WP_2 micro-particles, in the presence of co-catalyst element Pt, demonstrate remarkable photocatalytic H_2 generation performance under UV light irradiation as suggested by Pi et al. (Figs. 14e-g) [162]. Song et al. present a hybrid photocatalytic system comprising MoP-Cu_3P, with Cu_3P serving as an efficient photocatalyst. The MoP-Cu_3P photocatalyst demonstrates exceptional photocatalytic activity, with the H_2-production rate of 855 μmol h^{-1} g^{-1}, representing an improvement of 3.34 times compared to that of the bare Cu_3P (Figs. 14h-j) [163].

5. Conclusion and perspectives

In summary, this review comprehensively summarized the recent advancements in TMPs as co-catalysts for photocatalytic hydrogen production from water splitting. Firstly, we have provided a concise overview of the historical development and structural characteristics commonly found in TMPs. Then, we summarized the synthesis strategies of TMPs originating from various phosphorus sources, including phosphate, organophosphorus, phytic acid, NaH_2PO_2, red/black phosphorus, and so on. Furthermore, when employing these phosphorus sources as a means of supplying phosphorus for the formation of TMPs, an exhaustive analysis has been conducted to outline their inherent advantages and disadvantages. After that, we discussed the recent research endeavors of TMPs toward their capacity as photocatalytic co-catalysts for H_2 generation through photocatalysis. Moreover, the current photocatalytic H_2 evolution performance comparison over the above-described photocatalysts was analyzed and summarized in detail. At last, the present bottlenecks, challenges, and future research directions to enhance the activity of TMPs are highlighted.

Despite considerable developments in the photocatalytic H_2 evolution field that have been made for TMPs co-catalysts during the past decades, a summary of current challenges and prospects for future development are still urgently needed for further progress based on TMPs. According to the results of the above summary, some viewpoints are provided as follows:

(1) Currently, although kinds of methods are available for synthesizing TMPs, most preparation strategies still involve high reaction temperatures, requirements for dangerous gas handling, prolonged reaction times, etc. On the other hand, TMPs possess numerous phase variations with tiny stoichiometric differences. Therefore, how to obtain phase pure TMPs is still a tough challenge. Recently, several advanced synthesis technologies have been proposed for the acquisition of such TMPs, including ultrafast high-temperature sintering, flash joule heating, etc.

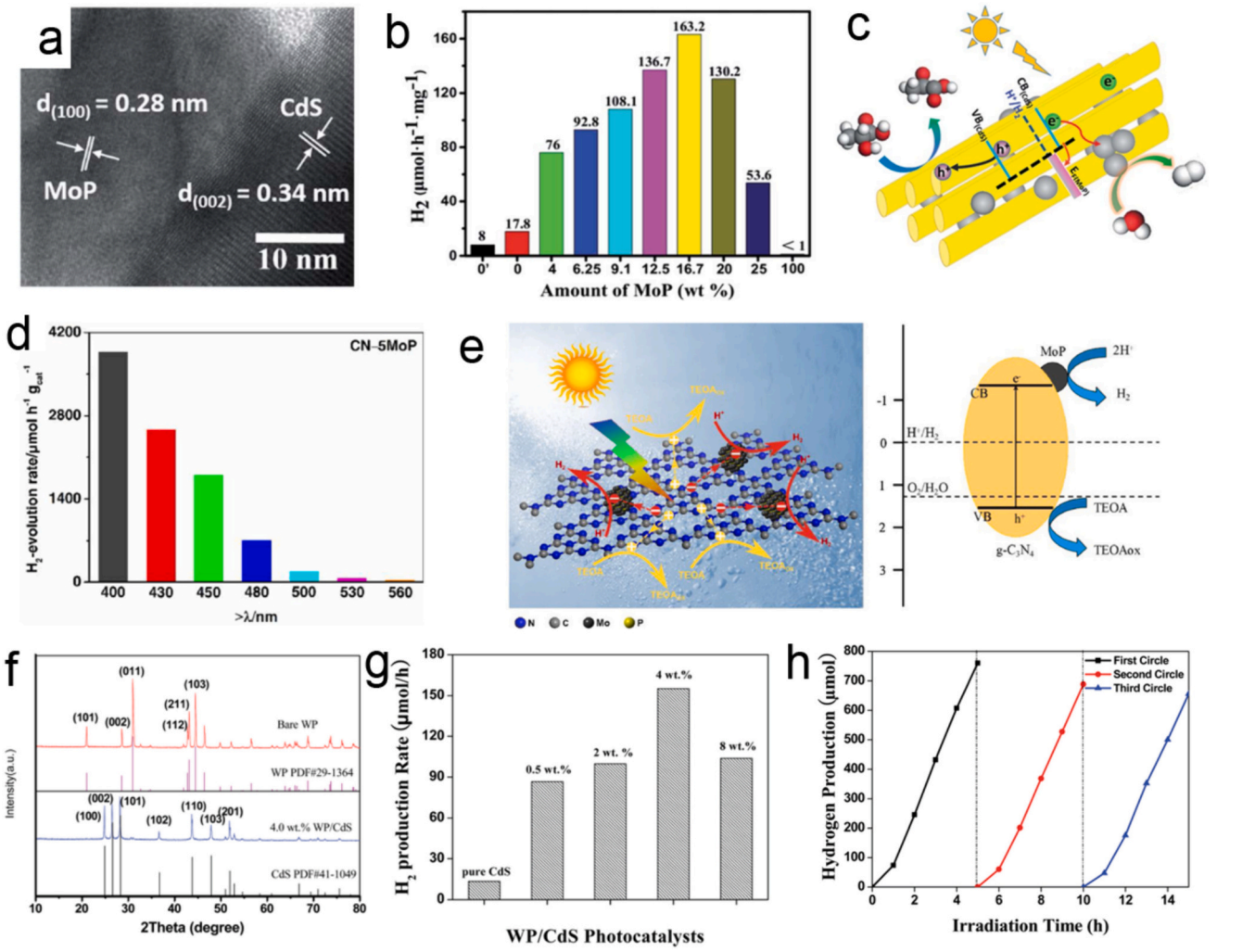

Fig. 12. (a) HRTEM image of MoP/CdS NRs. (b) H_2-production rate of MoP/CdS NR materials with varying MoP loading. (c) The photocatalytic mechanism of H_2 evolution using the MoP/CdS NR hybrid. Reprinted with permission from ref. 144. (d) Photocatalytic hydrogen evolution performance of C_3N_4 – MoP hybrid under various light spectra irradiation. (e) Schematic diagrams illustrating the proposed mechanism for MoP/g-C_3N_4 photocatalyst. Reprinted with permission from ref. 145. (f) XRD patterns of WP and WP/CdS. (g) Photocatalytic H_2-production from WP/CdS materials with different WP-loaded concentrations. (h) Repeatability of photocatalytic H_2-production via the WP/CdS photocatalyst. Reproduced with permission from ref. 150.

(2) Exploration of novel and highly efficient TMPs is currently a topic of great interest. Among the reported TMPs, those based on Fe/Co/Ni/Cu/Mo/W have demonstrated catalytic activity for photocatalytic H_2 generation but are still not high enough to reach the industrial level. Recently, some non-metal-based phosphides, such as boron phosphide, have been reported to be remarkably promising for use in photocatalyst for water splitting [164]. Further development of other groups of TMPs holds promising prospects for future applications.

(3) Currently, the combination of TMPs with commonly utilized materials such as TiO_2, CdS, and g-C_3N_4 has been extensively documented in the literature. The inclusion of other novel semiconductors, such as InGaN and AlGaN which offer adjustable band gaps ranging from 0.7 to 6.2 eV should also be considered in the future photocatalytic systems for a wide light response range.

(4) Currently, sacrificial agents are usually used to prevent the recombination of photogenerated electron-hole pairs by consuming photogenerated holes. However, the use of sacrificial agents can cause water pollution and limit sustainable practical applications. This issue can be addressed by combining HER with the degradation of organic contaminants or selective oxidation processes. In nother words, replacing sacrificial agents with organic contaminants or precursors of valuable chemical products is essential for future development.

(5) The majority of reported semiconductor photocatalysts/TMPs compound systems have been obtained through a simplified physical mixing approach, which inevitably leads to issues such as non-uniform mixtures. Future research should focus on developing a one-step method for simultaneous acquisition of both semiconductors (C_3N_4, etc.) and TMPs.

(6) Significant advancements have been achieved in recent years in the design of highly efficient photocatalysts. The instability of photocatalysts remains a significant challenge for practical applications. On one hand, future research should focus on developing an anti-photocorrosion layer and enhancing oxygen separation technology to effectively eliminate nascent oxygen and prevent oxygen-related photocorrosion. On the other hand, the stability of TMPs also should be enhanced under oxidation, acid, alkaline, etc. conditions. In this instance, the development of core-shell structures with TMPs as the core and corrosion-resistance nanoceramics (such as TiB_2, NbB_2, TaB_2, etc.) as the shell is a promising direction for improving the stability of the photocatalysts.

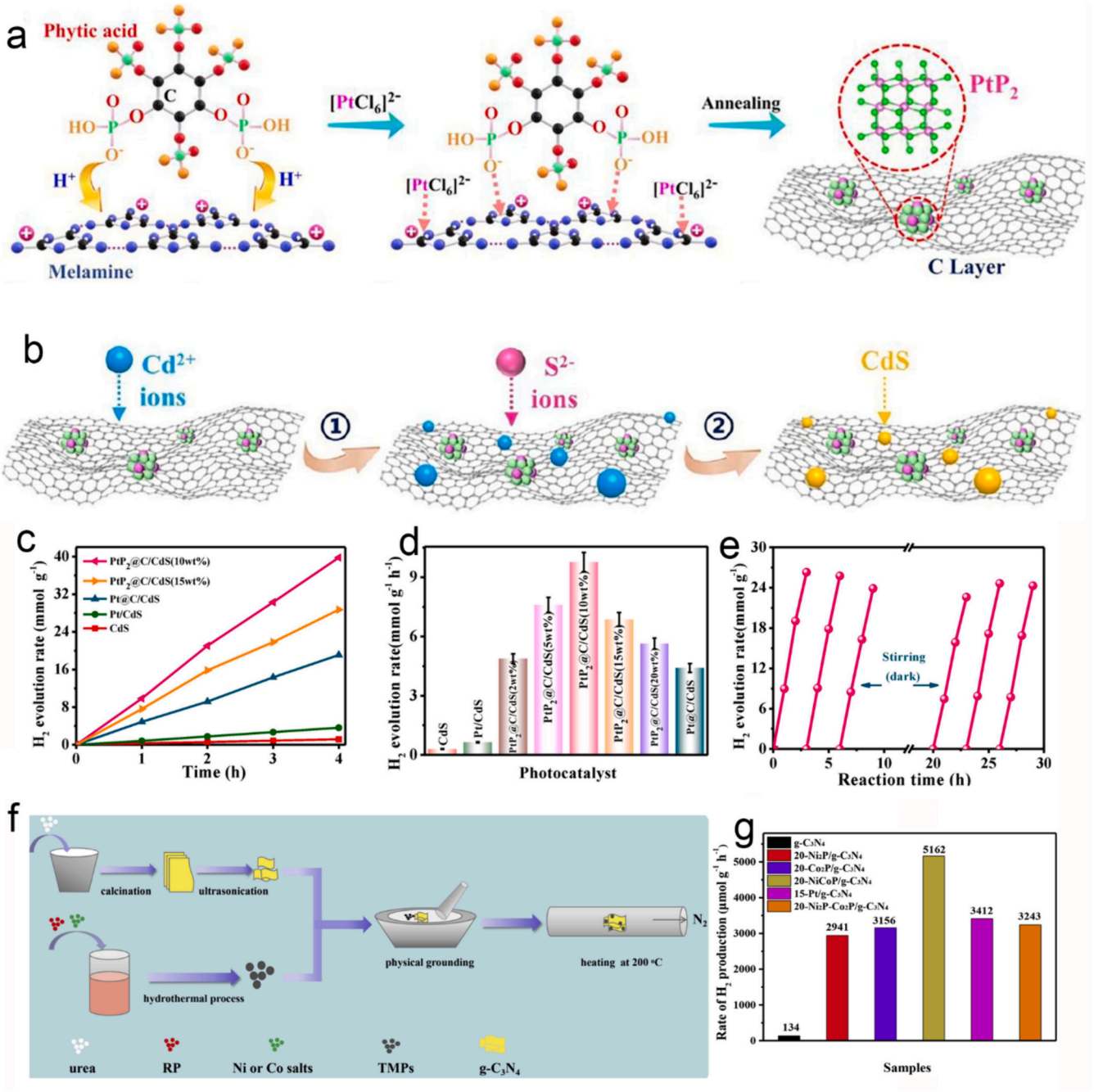

Fig. 13. Schematic representation of the synthetic procedure for (a) PtP_2@C and (b) PtP_2@C/CdS. (c) H_2 evolution (c) amount and (d) rate at different materials. (e) Cycling durability test of PtP_2@C/CdS. Reproduced with permission from ref. 156. (f) Schematic representation of the fabrication of NiCoP/g-C_3N_4 photocatalysts. (g) Comparison of photocatalytic H_2 production rates for the samples. Reproduced with permission from ref. 157.

(7) The investigations into the physicochemical properties, dynamics of photo-induced charge carriers, and mechanisms of H_2 evolution in loaded photocatalysts are currently limited. Therefore, the utilization of in-situ/operando characterization techniques, (e.g., X-ray absorption spectroscopy, Raman, transmission electron microscopy (TEM), X-ray photoelectron spectroscopy (XPS), infrared (IR) spectroscopy, etc.) and related theoretical modeling is important. These methods help to understand the catalysts in terms of the active sites, catalytic mechanisms, and degradation mechanisms at the molecular scale by integrating experimental findings.

(8) Current research on co-catalysts for TMPs is primarily focused on the half-reaction of H_2 evolution. The ultimate objective of developing highly efficient TMPs co-catalysts is to accomplish complete water splitting exclusively through the utilization of solar energy. Consequently, future investigations on the utilization of TMPs co-catalysts should be directed toward their applications in the field of overall water splitting.

Declaration of competing interest

The authors declare that they have no known competing financial interests or personal relationships that could be perceived as exerting any influence on the finding presented in this paper.

Table 1
Comparison of photocatalytic H_2-production performance of the TMPs co-catalysts in literature.

Catalyst	Co-catalyst	Phosphorus sources	Sacrificial agent	Light source	H_2 evolution rates	Apparent quantum efficiency	Stability	Ref.
CdS/o-Co_2P	Co_2P	Na_2HPO_2	lactic acid	Visible light	184.48 mmol g^{-1} h^{-1}	22.17%	~25 h	32
$Zn_xCd_{1-x}S/CoP_2$	CoP_2	$NaH_2PO_2{\cdot}H_2O$	lactic acid	λ = 400–550 nm	1244.3 μmol	–	40 h	37
$Co_2P/CdIn_2S_4$	Co_2P	$NaH_2PO_2{\cdot}H_2O$	lactic acid	λ ≥ 420 nm	471.9 μmol g^{-1} h^{-1}	–	15 h	119
Co_2P/S-CN	Co_2P	$(NH_4)_2HPO_4$	triethanolamine	λ = 400 nm	0.39 μmol·h^{-1}	–	50 h	118
CoP_x/CdS	CoP_x	Yellow phosphorus	Na_2SO_3 and Na_2S	λ= 450 nm	~500 mmol h^{-1} mg^{-1}	~35%	70 h	120
Red P/CoP_2/SiO_2	CoP_2	Red phosphorus	H_2O	Visible light (λ ≥ 420 nm) source	11.79 μmol h^{-1}	–	–	124
Fe_2P/S-CN	Fe_2P	$(NH_4)_2HPO_4$	triethanolamine	λ = 400 nm	0.32 μmol·h^{-1}	–	50 h	118
$Fe_2P/CdIn_2S_4$	Fe_2P	$NaH_2PO_2{\cdot}H_2O$	lactic acid	λ ≥ 420 nm	316.8 μmol h^{-1} g^{-1}	–	15 h	119
FeP/TiO_2	FeP	Tri-n-octylphosphine	Methanol	UV illumination	1.9 μmol H_2 mg^{-1} h^{-1}	~56%	16 h	123
Ni_2P/S-CN	Ni_2P	$(NH_4)_2HPO_4$	triethanolamine	λ = 400 nm	0.41 μmol·h^{-1}	–	50 h	118
$Ni_2P/CdIn_2S_4$	Ni_2P	$NaH_2PO_2{\cdot}H_2O$	lactic acid	λ ≥ 420 nm	810.0 μmol g^{-1} h^{-1}	–	15 h	119
Ni_2P/CdS	Ni_2P	Yellow phosphorous	Na_2SO_3 and Na_2S	Visible light irradiation	~1200 mmol h^{-1} mg^{-1}	~41%	12 h	102
Cu_3P/CdS	Cu_3P	Yellow phosphorus	Na_2SO_3 and Na_2S	λ >420	200 mmol h^{-1} mg^{-1}	~25%	12 h	125
Cu_3P/ZnS	Cu_3P	NaH_2PO_2	Na_2SO_3 and Na_2S	250 W QTH lamp	14,937 μmol h^{-1} g^{-1}	~44%	20 h	126
$Cu_3P/g\text{-}C_3N_4$	Cu_3P	NaH_2PO_2	–	λ = 420 nm	277.2 μmol h^{-1} g^{-1}	3.74%	10 h	127
p-type Cu_3P/n-type g-C_3N_4	Cu_3P	NaH_2PO_2	TEOA	300 W Xe lamp	808 μmol g^{-1} h^{-1}	–	18 h	122
MoP-400	MoP	$NaH_2PO_2{\cdot}H_2O$	Trimethylamine	λ ≥ 420 nm	~15 mmol h^{-1} g^{-1}	48%	16 h	141
MoP@MoO_3	MoP	NaH_2PO_2	TEOA	–	10,000.02 μmol h^{-1} g^{-1}	7.78%	35 h	142
MoP/CdS	MoP	$(NH_4)_2HPO_4$	lactic acid	λ > 420 nm	~163.2 mmol h^{-1} mg^{-1}	16.7%	54 h	144
MoP/g-C_3N_4	MoP	$NaH_2PO_2{\cdot}H_2O$	TEOA	λ > 400 nm	3868 μmol h^{-1} g_{cat}^{-1}	21.6%	20 h	145
MoP-Cu_3P	MoP	$NaH_2PO_2{\cdot}H_2O$	Na_2SO_3 and Na_2S	λ ≥ 420 nm	855 μmol h^{-1} g^{-1}	31%	24 h	163
WPS/CdS	WPS	$NaPO_2H_2{\cdot}H_2O$	lactic acid	–	~251.4 μmol g^{-1} h^{-1}	9.15%	25 h	146
WP/$ZnIn_2S_4$	WP	$NaPO_2H_2{\cdot}H_2O$	lactic acid	λ > 420 nm	1235 μmol g^{-1} h^{-1}	–	20 h	147
Pd/WP/CdS	WP	$(NH_4)_2HPO_4$	lactic acid	λ = 420 nm	18.0 mmol h^{-1} g^{-1}	11.8%	10 h	149
WP/CdS	WP	$(NH_4)_2HPO_4$	$(NH_4)_2SO_3$	λ = 420 nm	155.2 μmol h^{-1}	10.5%	15 h	150
RuP/g-C_3N_4	RuP	$NaH_2PO_2{\cdot}H_2O$	TEOA	λ > 400 nm	2110 μmol h^{-1} g^{-1}	–	20 h	151
Ru_xP/P-doped g-C_3N_4	Ru_xP	NaH_2PO_2	TEOA	300 W Xe lamp	1.94 mmol g^{-1} h^{-1}	0.2%	450 min	152
RhP/g-C_3N_4	RhP	NaH_2PO_2	TEOA	300 W Xe lamp	41.57 μmol h^{-1}	–	16 h	154
$Rh_xP/g\text{-}C_3N_4$	Rh_xP	NaH_2PO_2	TEOA	λ = 420 nm	3055.9 μmol h^{-1} g^{-1}	18.4%	104 h	155
PtP_2@C/CdS	PtP_2	Phytic acid	lactic acid	λ = 420 nm	9.76 mmol g^{-1} h^{-1}	41.67%	~30 h	156
NiCoP/CdS	NiCoP	NaH_2PO_2	Methanol	λ >420 nm	708 mmol h^{-1}	45.5%	18 h	121
NiCoP/g-C_3N_4	NiCoP	Red phosphorus	TEOA	400 nm	5162 μmol g^{-1} h^{-1}	18.5%	12 h	157
NiFeP/g-C_3N_4	NiFeP	NaH_2PO_2	TEOA	300 W Xe lamp	3.549 mmol g^{-1} h^{-1}	4.98%	540 h	158
$Mn_{0.67}Co_{1.33}P$ /g-C_3N_4	$Mn_{0.67}Co_{1.33}P$	NaH_2PO_2	TEOA	300 W Xe lamp	113.1 μmol h^{-1}	4.7%	20 h	159
Cu_3P-Ni_2P /g-C_3N_4	Cu_3P-Ni_2P	Red phosphorus	TEOA	λ = 400 nm	6529.8 μmol g^{-1} h^{-1}	18.5%	15 h	160

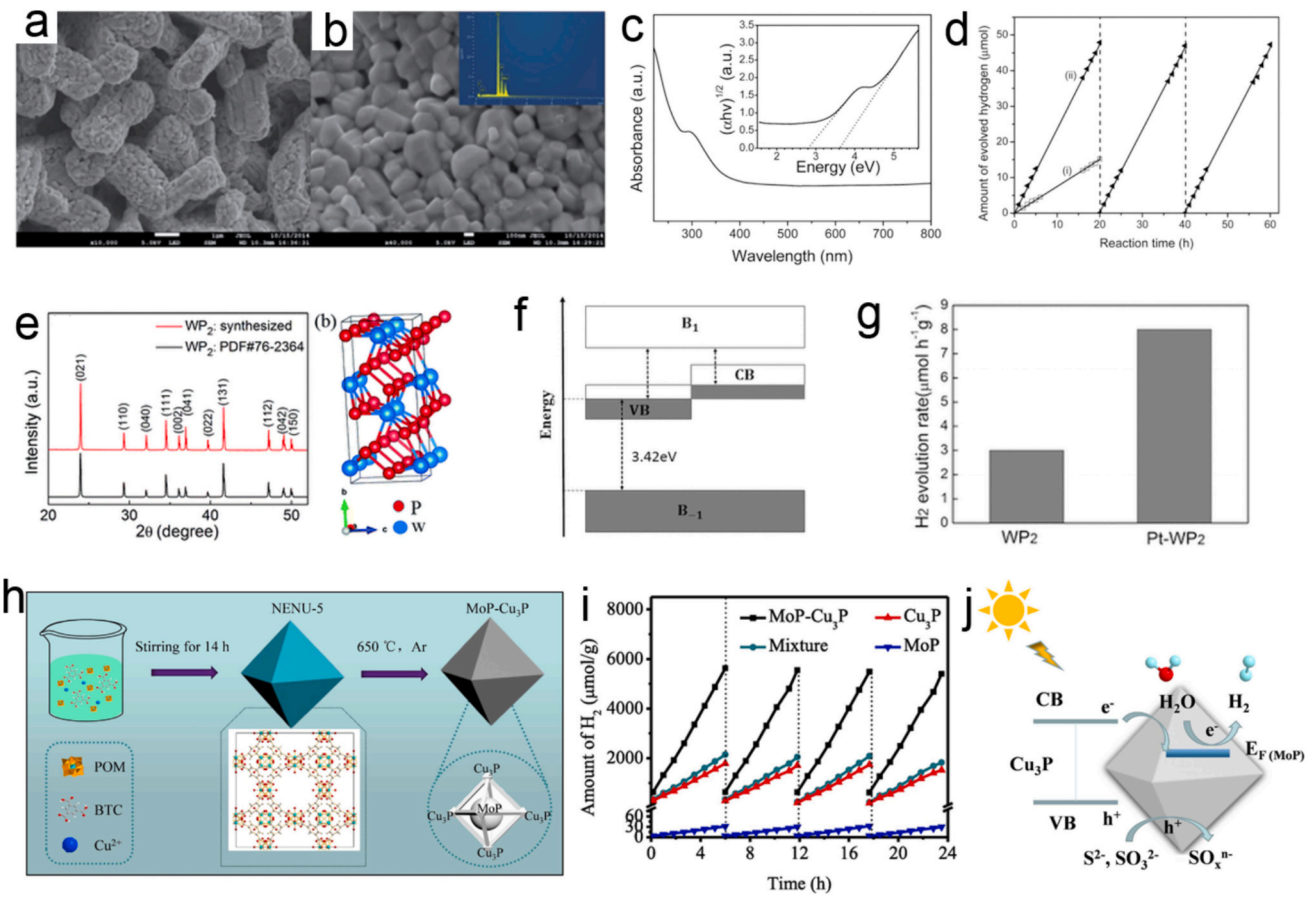

Fig. 14. (a, b) SEM images of MoP_2 nanoparticles. (c) UV–vis absorption spectrum of the MoP_2 powder. (d) H_2-generation from H_2O using MoP_2 as the photocatalyst. Reproduced with permission from ref. 161. (e) XRD patterns and crystal structure of WP_2. (f) Schematic band structure and transition mechanism of WP_2. (g) Hydrogen evolution rate of WP_2 and 2% Pt–WP_2. Reproduced with permission from ref. 162. (h) Scheme of the fabrication process of MoP-Cu_3P hybrids. (i) Photocatalytic H_2-production activity of the MoP, Cu_3P, mixture, and MoP-Cu_3P hybrids. (j) The photocatalytic H_2 evolution mechanism by MoP-Cu_3P hybrids materials. Reproduced with permission from ref. 163.

Data availability

Data will be made available on request.

Acknowledgements

This work was supported financially by the Natural Sciences and Engineering Research Council of Canada (NSERC), Institut National de la Recherche Scientifique (INRS), École de Technologie Supérieure (ÉTS) and Fujian Province Young and Middle-Aged Teacher Education Research Project (JZ230009). Dr. G. Zhang thanks for the support from the Marcelle-Gauvreau Engineering Research Chair program. Dr. A.M. Al-Enizi and Dr. Z. Pu extend their sincere appreciation to the Distinguished Scientist Fellowship Program (DSFP) at King Saud University for funding of this work.

References

[1] L. Schlapbach, A. Züttel, Nature 414 (2001) 353–358.
[2] X. Lv, W. Tian, Z. Yuan, Electrochem. Energy Rev. 6 (2023) 23.
[3] A. Fujishima, K. Honda, Nature 238 (1972) 37–38.
[4] S. Cao, L. Piao, X. Chen, Trends Chem. 2 (2020) 57–70.
[5] Y. Liu, F. Wang, Z. Jiao, S. Bai, H. Qiu, L. Guo, Electrochem. Energy Rev. 5 (2022) 5.
[6] Z. Chen, G. Zhang, J. Prakash, Y. Zheng, S. Sun, Adv. Energy Mater. 9 (2019) 1900889.
[7] J. Zhu, P. Li, W. Guo, Y. Zhao, R. Zou, Coordin, Chem. Rev. 359 (2018) 80–101.
[8] H. Zhang, L.V. Besteiro, J. Liu, C. Wang, G.S. Selopal, Z. Chen, D. Barba, Z. M. Wang, H. Zhao, G.P. Lopinski, Nano Energy 79 (2021) 105416.
[9] X. Chen, S. Shen, L. Guo, S.S. Mao, Chem. Rev. 110 (2010) 6503–6570.
[10] K.A. Adegoke, M. Iqbal, H. Louis, S.U. Jan, A. Mateen, O.S. Bello, Pak. J. Anal. Environ. Chem. 19 (2018) 1–27.
[11] F. Chen, T. Ma, T. Zhang, Y. Zhang, H. Huang, Adv. Mater. 33 (2021) 2005256.
[12] Q. Liu, Z. Wang, H. Chen, H.Y. Wang, H. Song, J. Ye, Y. Weng, ChemCatChem 12 (2020) 3838–3842.
[13] Y. Zhao, Z. Niu, J. Zhao, L. Xue, X. Fu, J. Long, Electrochem. Energy Rev. 12 (2023) 14.
[14] S. Cao, Y. Li, B. Zhu, M. Jaroniec, J. Yu, J. Catal. 349 (2017) 208–217.
[15] M. Liu, P. Xia, L. Zhang, B. Cheng, J. Yu, ACS Sustain. Chem. Eng. 6 (2018) 10472–10480.
[16] J. Wang, Z. Guan, J. Huang, Q. Li, J. Yang, J. Mater. Chem. A 2 (2014) 7960–7966.
[17] W.R. McNamara, Z. Han, C.-J. Yin, W.W. Brennessel, P.L. Holland, R. Eisenberg, Proc. Natl. Acad. Sci. 109 (2012) 15594–15599.
[18] T. Peng, X. Zhang, P. Zeng, K. Li, X. Zhang, X. Li, J. Catal. 303 (2013) 156–163.
[19] L. Liu, H. Zhao, J.M. Andino, Y. Li, ACS Catal. 2 (2012) 1817–1828.
[20] J.A. Torres, A.E. Nogueira, G.T. da Silva, O.F. Lopes, Y. Wang, T. He, C. Ribeiro, J. CO_2 Util. 35 (2020) 106–114.
[21] R.M. Irfan, M.H. Tahir, M. Maqsood, Y. Lin, T. Bashir, S. Iqbal, J. Zhao, L. Gao, M. Haroon, J. Catal. 390 (2020) 196–205.
[22] L. Wei, Y. Chen, Y. Lin, H. Wu, R. Yuan, Z. Li, Appl. Catal. B Environ. 144 (2014) 521–527.
[23] R.K. Chava, T. Kim, Y. Kim, M. Kang, J. Mater. Chem. C 11 (2023) 1782–1790.
[24] Z. Jin, T. Wei, F. Li, Q. Zhang, L. Xu, New J. Chem. 44 (2020) 3471–3477.
[25] M. Chen, S. Li, S. Zhong, X. Zhou, Y. Ge, J. Luo, X. Zhou, X. Zhou, Y. Zhong, J. Alloys Compd. 947 (2023) 169515.
[26] J. Di, C. Chen, C. Zhu, P. Song, M. Duan, J. Xiong, R. Long, M. Xu, L. Kang, S. Guo, Nano Energy 79 (2021) 105429.
[27] B. Ma, H. Xu, K. Lin, J. Li, H. Zhan, W. Liu, C. Li, ChemSusChem 9 (2016) 820–824.
[28] Y. Chen, W. Gu, L. Tan, Z. Ao, T. An, S. Wang, Appl. Catal. A-Gen. 618 (2021) 118127.
[29] Y. Dang, L. Feng, W. Hu, W. Wang, Q. Zhang, B. Ma, Int. J. Hydrog. Energy 46 (2021) 39251–39261.
[30] R.M. Irfan, M.H. Tahir, S. Iqbal, M. Nadeem, T. Bashir, M. Maqsood, J. Zhao, L. Gao, J. Mater. Chem. C 9 (2021) 3145–3154.

[31] P. Ye, X. Liu, J. Iocozzia, Y. Yuan, L. Gu, G. Xu, Z. Lin, J. Mater. Chem. A 5 (2017) 8493–8498.
[32] Y. Chao, J. Zheng, H. Zhang, F. Li, F. Yan, Y. Tan, Z. Zhu, Chem. Eng. J. 346 (2018) 281–288.
[33] M. Ashraf, N. Ullah, F. Raziq, I. Khan, K.R. Alhooshani, S.A. Ganiyu, M.N. Tahir, Electrochim. Acta 470 (2023) 143296.
[34] L. Luo, J. Tian, W. Hu, P. Han, W. Wang, B. Ma, Appl. Catal. B Environ. 321 (2023) 122008.
[35] G. Yan, X. Sun, K. Zhang, Y. Zhang, H. Li, Y. Dou, D. Yuan, H. Huang, B. Jia, H. Li, Small 18 (2022) 2201340.
[36] C. Li, D. Zhu, S. Cheng, Y. Zuo, Y. Wang, C. Ma, H. Dong, Chin. Chem. Lett. 33 (2022) 1141–1153.
[37] X. Guo, C. Chang, G. Wang, X. Hao, Z. Jin, Adv. Sustain. Syst. 7 (2023) 2200189.
[38] S. Carenco, D. Portehault, C. Boissiere, N. Mezailles, C. Sanchez, Chem. Rev. 113 (2013) 7981–8065.
[39] N.P. Sweeny, C.S. Rohrer, O. Brown, J. Am. Chem. Soc. 80 (1958) 799–800.
[40] Y. Xu, R. Wu, J. Zhang, Y. Shi, B. Zhang, Chem. Commun. 49 (2013) 6656–6658.
[41] E.J. Popczun, J.R. McKone, C.G. Read, A.J. Biacchi, A.M. Wiltrout, N.S. Lewis, R. E. Schaak, J. Am. Chem. Soc. 135 (2013) 9267–9270.
[42] S. Xu, H. Zhao, T. Li, J. Liang, S. Lu, G. Chen, S. Gao, A.M. Asiri, Q. Wu, X. Sun, J. Mater. Chem. A 8 (2020) 19729–19745.
[43] Z. Pu, Q. Liu, P. Jiang, A.M. Asiri, A.Y. Obaid, X. Sun, Chem. Mater. 26 (2014) 4326–4329.
[44] Z. Pu, Q. Liu, A.M. Asiri, X. Sun, ACS Appl. Mater. Interfaces 6 (2014) 21874–21879.
[45] T. Liu, D. Liu, F. Qu, D. Wang, L. Zhang, R. Ge, S. Hao, Y. Ma, G. Du, A.M. Asiri, Adv. Energy Mater. 7 (2017) 1700020.
[46] Z. Pu, T. Liu, I.S. Amiinu, R. Cheng, P. Wang, C. Zhang, P. Ji, W. Hu, J. Liu, S. Mu, Adv. Funct. Mater. 30 (2020) 2004009.
[47] S.T. Oyama, T. Gott, H. Zhao, Y.-K. Lee, Catal. Today 143 (2009) 94–107.
[48] Y. Shi, B. Zhang, Chem. Soc. Rev. 45 (2016) 1529–1541.
[49] P. Xiao, M. Sk, L. Thia, X. Ge, R. Lim, J. Wang, K. Lim, X. Wang, Angew. Chem. Int. Ed. 53 (2014) 14433–14437.
[50] J.F. Callejas, C.G. Read, C.W. Roske, N.S. Lewis, R.E. Schaak, Chem. Mater. 28 (2016) 6017–6044.
[51] Y. Shi, M. Li, Y. Yu, B. Zhang, Energy Environ. Sci. 13 (2020) 4564–4582.
[52] R. Blaugher, J. Hulm, P. Yocom, J. Phys. Chem. Solids 26 (1965) 2037–2039.
[53] J.-H. Chen, K.H. Whitmire, Coord. Chem. Rev. 355 (2018) 271–327.
[54] Z. Pu, I.S. Amiinu, M. Wang, Y. Yang, S. Mu, Nanoscale 8 (2016) 8500–8504.
[55] Z. Pu, J. Zhao, I.S. Amiinu, W. Li, M. Wang, D. He, S. Mu, Energy Environ. Sci. 12 (2019) 952–957.
[56] P. Ji, H. Jin, H. Xia, X. Luo, J. Zhu, Z. Pu, S. Mu, ACS Appl. Mater. Interfaces 12 (2019) 727–733.
[57] Z. Pu, I.S. Amiinu, Z. Kou, W. Li, S. Mu, Angew. Chem. Int. Ed. 56 (2017) 11559–11564.
[58] Q. Sheng, X. Li, R. Prins, C. Liu, Q. Hao, S. Chen, Angew. Chem. Int. Ed. 60 (2021) 11180–11183.
[59] Z. Xing, Q. Liu, A.M. Asiri, X. Sun, Adv. Mater. 26 (2014) 5702–5707.
[60] Z. Pu, X. Ya, I.S. Amiinu, Z. Tu, X. Liu, W. Li, S. Mu, J. Mater. Chem. A 4 (2016) 15327–15332.
[61] Z. Pu, I.S. Amiinu, C. Zhang, M. Wang, Z. Kou, S. Mu, Nanoscale 9 (2017) 3555–3560.
[62] H. Li, S.M. Xu, H. Yan, L. Yang, S. Xu, Small 14 (2018) 1800367.
[63] Z. Zhao, Y. Duan, F. Chen, Z. Tian, R. Pathak, J.W. Elam, Z. Yi, Y. Wang, X. Wang, Chem. Eng. J. 450 (2022) 138310.
[64] P. Wei, X. Sun, Z. He, F. Cheng, J. Xu, Q. Li, Y. Ren, J. He, J. Han, Y. Huang, Fuel 339 (2023) 127303.
[65] J. Park, B. Koo, Y. Hwang, C. Bae, K. An, J.G. Park, H.M. Park, T. Hyeon, Angew. Chem. Int. Ed. 116 (2004) 2332–2335.
[66] K. Wang, B. Huang, F. Lin, F. Lv, M. Luo, P. Zhou, Q. Liu, W. Zhang, C. Yang, Y. Tang, Adv. Energy Mater. 8 (2018) 1801891.
[67] K. Sun, M. Liu, J. Pei, D. Li, C. Ding, K. Wu, H.L. Jiang, Angew. Chem. Int. Ed. 132 (2020) 22937–22943.
[68] X. Li, W. Xing, T. Hu, K. Luo, J. Wang, W. Tang, Coord. Chem. Rev. 473 (2022) 214811.
[69] D. Liu, A. Wang, C. Liu, R. Prins, Catal. Today 292 (2017) 133–142.
[70] A. Sumboja, T. An, H.Y. Goh, M. Lübke, D.P. Howard, Y. Xu, A.D. Handoko, Y. Zong, Z. Liu, ACS Appl. Mater. Interfaces 10 (2018) 15673–15680.
[71] L. Yue, J. Liang, Z. Wu, B. Zhong, Y. Luo, Q. Liu, T. Li, Q. Kong, Y. Liu, A.M. Asiri, J. Mater. Chem. A 9 (2021) 11879–11907.
[72] J. Tian, Q. Liu, N. Cheng, A.M. Asiri, X. Sun, Angew. Chem. Int. Ed. 126 (2014) 9731–9735.
[73] C. Tang, R. Zhang, W. Lu, L. He, X. Jiang, A.M. Asiri, X. Sun, Adv. Mater. 29 (2017) 1602441.
[74] X. Yu, S. Xu, Z. Wang, X. Cheng, Y. Du, G. Chen, X. Sun, Q. Wu, Nanoscale 13 (2021) 11069–11076.
[75] I.A. Liyanage, A.V. Flores, E.G. Gillan, Inorg. Chem. 62 (2023) 4947–4959.
[76] H. Bai, D. Chen, Q. Ma, R. Qin, H. Xu, Y. Zhao, J. Chen, S. Mu, Electrochem. Energy Rev. 5 (2022) 24.
[77] A. Ali, F. Long, P. Shen, Electrochem. Energy Rev. 5 (2022) 1.
[78] D. Chen, Z. Pu, R. Lu, P. Ji, P. Wang, J. Zhu, C. Lin, H.W. Li, X. Zhou, Z. Hu, Adv. Energy Mater. 10 (2020) 2000814.
[79] Y. Zhao, N. Jia, X.-R. Wu, F.-M. Li, P. Chen, P.-J. Jin, S. Yin, Y. Chen, Appl. Catal. B Environ. 270 (2020) 118880.
[80] J.Q. Chi, X.J. Zeng, X. Shang, B. Dong, Y.M. Chai, C.G. Liu, M. Marin, Y. Yin, Adv. Funct. Mater. 29 (2019) 1901790.
[81] S.B. Roy, S. Moon, A. Patil, M.A. Rehman, S. Yoo, Y. Seo, J.H. Park, K. Kang, S. C. Jun, Appl. Catal. B Environ. 319 (2022) 121906.
[82] Z. Pu, Q. Liu, C. Tang, A.M. Asiri, X. Sun, Nanoscale 6 (2014) 11031–11034.
[83] W. Zhu, C. Tang, D. Liu, J. Wang, A.M. Asiri, X. Sun, J. Mater. Chem. A 4 (2016) 7169–7173.
[84] T. Liu, S. Wang, Q. Zhang, L. Chen, W. Hu, C.M. Li, Chem. Commun. 54 (2018) 3343–3346.
[85] J. Fan, L. Wang, X. Xiang, Y. Liu, N. Shi, Y. Lin, D. Xu, J. Jiang, Y. Lai, J. Bao, M. Han, Small Methods 8 (2024) 2301279.
[86] H. Song, Y. Cheng, B. Li, Y. Fan, B. Liu, Z. Tang, S. Lu, ACS Sustain. Chem. Eng. 8 (2020) 3995–4002.
[87] H. Liang, A.N. Gandi, D.H. Anjum, X. Wang, U. Schwingenschlögl, H.N. Alshareef, Nano Lett. 16 (2016) 7718–7725.
[88] C. Zhang, Z. Pu, I.S. Amiinu, Y. Zhao, J. Zhu, Y. Tang, S. Mu, Nanoscale 10 (2018) 2902–2907.
[89] Z. Pu, T. Liu, W. Zhao, X. Shi, Y. Liu, G. Zhang, W. Hu, S. Sun, S. Liao, ACS Appl. Mater. Interfaces 12 (2020) 11737–11744.
[90] J. Zhao, Z. Pu, H. Jin, Z. Zhang, J. Liu, S. Mu, J. Catal. 383 (2020) 244–253.
[91] Z. Pu, R. Cheng, J. Zhao, Z. Hu, C. Li, W. Li, P. Wang, I.S. Amiinu, Z. Wang, M. Wang, iScience 23 (2020) 101793.
[92] Z. Pu, I.S. Amiinu, D. He, M. Wang, G. Li, S. Mu, Nanoscale 10 (2018) 12407–12412.
[93] X. Wang, Z. Na, D. Yin, C. Wang, Y. Wu, G. Huang, L. Wang, ACS Nano 12 (2018) 12238–12246.
[94] X.F. Lu, L. Yu, X.W. Lou, Sci. Adv. 5 (2019) eaav6009.
[95] Y.-J. Yuan, Z.-K. Shen, S. Song, J. Guan, L. Bao, L. Pei, Y. Su, S. Wu, W. Bai, Z.-T. Yu, ACS Catal. 9 (2019) 7801–7807.
[96] A. Chouat, D.T. Nguyen, S. Mohan, T.O. Do, ACS Appl. Nano Mater. 5 (2022) 13078–13089.
[97] Q. Liang, F. Shi, X. Xiao, X. Wu, K. Huang, S. Feng, ChemCatChem 10 (2018) 2179–2183.
[98] Y. Xu, W. Zhang, G. Zhou, M. Jin, X. Li, J. Colloid Interface Sci. 616 (2022) 641–648.
[99] Z.-K. Shen, M. Cheng, Y.-J. Yuan, L. Pei, J. Zhong, J. Guan, X. Li, Z.-J. Li, L. Bao, X. Zhang, Appl. Catal. B Environ. 295 (2021) 120274.
[100] T. Wu, Y. Dang, J. He, T. Li, G. Qu, Y. Gao, F. Tan, Appl. Surf. Sci. 494 (2019) 179–186.
[101] T. Bao, A. Bolag, X. Tian, T. Ojiyed, Crystals 13 (2023) 1571.
[102] Z. Sun, H. Zheng, J. Li, P. Du, Energy Environ. Sci. 8 (2015) 2668–2676.
[103] D.E. Schipper, Z. Zhao, H. Thirumalai, A.P. Leitner, S.L. Donaldson, A. Kumar, F. Qin, Z. Wang, L.C. Grabow, J. Bao, Chem. Mater. 30 (2018) 3588–3598.
[104] B. Weng, X. Wang, C.R. Grice, F. Xu, Y. Yan, J. Mater. Chem. A 7 (2019) 7168–7178.
[105] Z. Lu, L. Sepunaru, Electrochim. Acta 363 (2020) 137167.
[106] L. Chai, S. Liu, S. Pei, C. Wang, Chem. Eng. J. 420 (2021) 129686.
[107] J. Kim, H. Kim, S.H. Ahn, ACS Sustain. Chem. Eng. 7 (2019) 14041–14050.
[108] J. Yu, B. Chang, W. Yu, X. Li, D. Wang, Z. Xu, X. Zhang, H. Liu, W. Zhou, Carbon Energy 4 (2022) 237–245.
[109] G. Li, J. Yu, J. Jia, L. Yang, L. Zhao, W. Zhou, H. Liu, Adv. Funct. Mater. 28 (2018) 1801332.
[110] Y. Deng, L. Yang, Y. Wang, L. Zeng, J. Yu, B. Chen, X. Zhang, W. Zhou, Chin. Chem. Lett. 32 (2021) 511–515.
[111] J. Yu, G. Li, H. Liu, L. Zhao, A. Wang, Z. Liu, H. Li, H. Liu, Y. Hu, W. Zhou, Adv. Funct. Mater. 29 (2019) 1901154.
[112] G. Li, J. Wang, J. Yu, H. Liu, Q. Cao, J. Du, L. Zhao, J. Jia, H. Liu, W. Zhou, Appl. Catal. B Environ. 261 (2020) 118147.
[113] S. Yang, G. Chen, A.G. Ricciardulli, P. Zhang, Z. Zhang, H. Shi, J. Ma, J. Zhang, P. W. Blom, X. Feng, Angew. Chem. Int. Ed. 59 (2020) 465–470.
[114] S. Anantharaj, S.R. Ede, K. Sakthikumar, K. Karthick, S. Mishra, S. Kundu, ACS Catal. 6 (2016) 8069–8097.
[115] J. Hao, K. Wu, C. Lyu, Y. Yang, H. Wu, J. Liu, N. Liu, W.-M. Lau, J. Zheng, Mater. Horiz. 10 (2023) 2312–2342.
[116] X. Chen, J. Liu, T. Yuan, Z. Zhang, C. Song, S. Yang, X. Gao, N. Wang, L. Cui, Energy Mater. 2 (2022) 200028.
[117] P. Luo, Z. Pang, Z. Qin, T. Wei, S. Li, Y. Hu, C. Wei, Int. J. Hydrog. Energy 45 (2020) 28240–28251.
[118] Z. Sun, M. Zhu, X. Lv, Y. Liu, C. Shi, Y. Dai, A. Wang, T. Majima, Appl. Catal. B Environ. 246 (2019) 330–336.
[119] X. Ma, W. Li, C. Ren, M. Dong, L. Geng, T. Wang, Sep. Purif. Technol. 316 (2023) 123805.
[120] Z. Sun, B. Lv, J. Li, M. Xiao, X. Wang, P. Du, J. Mater. Chem. A 4 (2016) 1598–1602.
[121] H. Cao, T. Wang, A.C. Minja, D. Jiang, P. Du, Int. J. Hydrog. Energy 46 (2021) 32435–32444.
[122] T. Wang, L. Yang, D. Jiang, H. Cao, A.C. Minja, P. Du, ACS Appl. Mater. Interfaces 13 (2021) 23751–23759.
[123] J.F. Callejas, J.M. McEnaney, C.G. Read, J.C. Crompton, A.J. Biacchi, E. J. Popczun, T.R. Gordon, N.S. Lewis, R.E. Schaak, ACS Nano 8 (2014) 11101–11107.
[124] C. Yang, Y. Zhu, Y. Liu, H. Wang, D. Yang, J. Mater. Sci. Technol. 125 (2022) 59–66.
[125] Z. Sun, Q. Yue, J. Li, J. Xu, H. Zheng, P. Du, J. Mater. Chem. A 3 (2015) 10243–10247.
[126] R. Rameshbabu, P. Ravi, G. Pecchi, E.J. Delgado, R. Mangalaraja, M. Sathish, J. Colloid Interface Sci. 590 (2021) 82–93.

[127] W. Wang, X. Zhao, Y. Cao, Z. Yan, R. Zhu, Y. Tao, X. Chen, D. Zhang, G. Li, D. L. Phillips, ACS Appl. Mater. Interfaces 11 (2019) 16527–16537.
[128] A. Ioannidi, A. Petala, Z. Frontistis, J. Environ. Chem. Eng. 8 (2020) 104340.
[129] X. Zhang, D. Kim, J. Yan, L. Lee, ACS Appl. Mater. Interfaces 13 (2021) 9762–9770.
[130] L. Shi, J. Yin, Y. Liu, H. Liu, H. Zhang, H. Tang, Chemosphere 309 (2022) 136607.
[131] H. Zhou, R. Chen, C. Han, P. Wang, Z. Tong, B. Tan, Y. Huang, Z. Liu, J. Colloid Interface Sci. 610 (2022) 126–135.
[132] S. Hua, D. Qu, L. An, W. Jiang, Y. Wen, X. Wang, Z. Sun, Appl. Catal. B Environ. 240 (2019) 253–261.
[133] Z. Pu, T. Liu, G. Zhang, X. Liu, M.A. Gauthier, Z. Chen, S. Sun, Small Methods 5 (2021) 2100699.
[134] I.S. Amiinu, Z. Pu, X. Liu, K.A. Owusu, H.G.R. Monestel, F.O. Boakye, H. Zhang, S. Mu, Adv. Funct. Mater. 27 (2017) 1702300.
[135] Z. Pu, S. Wei, Z. Chen, S. Mu, Appl. Catal. B Environ. 196 (2016) 193–198.
[136] Z. Pu, Q. Liu, A.M. Asiri, Y. Luo, X. Sun, Y. He, Electrochim. Acta 168 (2015) 133–138.
[137] T. Wang, P. Wang, Y. Pang, Y. Wu, J. Yang, H. Chen, X. Gao, S. Mu, Z. Kou, Nano Res. 15 (2022) 3946–3951.
[138] Z. Zhang, J. Zhao, M. Wu, Q. Lu, R. Liu, Nano Res. 16 (2023) 4706–4714.
[139] C. Zhang, Z. Guo, Y. Tian, C. Yu, K. Liu, L. Jiang, Nano Res. Energy 2 (2023) e9120063.
[140] P. Xiao, M.A. Sk, L. Thia, X. Ge, R.J. Lim, J.-Y. Wang, K.H. Lim, X. Wang, Energy Environ. Sci. 7 (2014) 2624–2629.
[141] J. Xu, Y. Liu, J. Tan, Y. Li, S. Peng, W. Zhang, Inter. J. Hydrogen, Energy 47 (2022) 3814–3823.
[142] L. Zhang, Z. Jin, N. Tsubaki, Nanoscale 13 (2021) 18507–18519.
[143] Y. Huang, X. Song, J. Deng, C. Zha, W. Huang, Y. Wu, Y. Li, Appl. Catal. B Environ. 245 (2019) 656–661.
[144] Q. Yue, Y. Wan, Z. Sun, X. Wu, Y. Yuan, P. Du, J. Mater. Chem. A 3 (2015) 16941–16947.
[145] C. Cheng, S. Zong, J. Shi, F. Xue, Y. Zhang, X. Guan, B. Zheng, J. Deng, L. Guo, Appl. Catal. B Environ. 265 (2020) 118620.
[146] Q. Jian, X. Hao, Z. Jin, Q. Ma, Phys. Chem. Chem. Phys. 22 (2020) 1932–1943.
[147] X. Hao, Y. Shao, D. Xiang, Z. Jin, Adv. Mater. Interfaces 9 (2022) 2200185.
[148] X. Zhang, J. Yan, F. Zheng, J. Zhao, L. Lee, Appl. Catal. B Environ. 286 (2021) 119879.
[149] Y. Dang, J. Tian, W. Wang, B. Ma, J. Colloid Interface Sci. 633 (2023) 649–656.
[150] J. Zhang, W. Yao, C. Huang, P. Shi, Q. Xu, J. Mater. Chem. A 5 (2017) 12513–12519.
[151] J. Wang, J. Chen, P. Wang, J. Hou, C. Wang, Y. Ao, Appl. Catal. B Environ. 239 (2018) 578–585.
[152] J. Zhang, Q. Zhu, Y. Ma, L. Wang, M. Nasir, J. Zhang, Catal. Today 380 (2021) 223–229.
[153] Y. Gao, Y. Zhao, H. Liu, M. Shao, Z. Chen, T. Ma, Z. Wu, L. Wang, J. Colloid Interface Sci. 606 (2022) 1874–1881.
[154] Z. Chen, Y. Bu, L. Wang, X. Wang, J.-P. Ao, Appl. Catal. B Environ. 274 (2020) 119117.
[155] H. Dong, M. Xiao, S. Yu, H. Wu, Y. Wang, J. Sun, G. Chen, C. Li, ACS Catal. 10 (2019) 458–462.
[156] J. Xu, W. Zhong, D. Gao, X. Wang, P. Wang, H. Yu, Chem. Eng. J. 439 (2022) 135758.
[157] C. Jin, C. Xu, W. Chang, X. Ma, X. Hu, E. Liu, J. Fan, J. Alloys Compd. 803 (2019) 205–215.
[158] Q. Zhu, B. Qiu, H. Duan, Y. Gong, Z. Qin, B. Shen, M. Xing, J. Zhang, Appl. Catal. B Environ. 259 (2019) 118078.
[159] J. Wu, C. Li, W. Zhang, J. Han, L. Wang, S. Wang, Y. Wang, Energ. Technol. 7 (2019) 1800927.
[160] W. Sun, Z. Fu, H. Shi, C. Jin, E. Liu, X. Zhang, J. Fan, J. Chem. Technol. Biotechnol. 95 (2020) 3117–3125.
[161] T. Wu, S. Chen, D. Zhang, J. Hou, J. Mater. Chem. A 3 (2015) 10360–10367.
[162] M. Pi, T. Wu, D. Zhang, S. Chen, S. Wang, RSC Adv. 6 (2016) 15724–15730.
[163] Y. Song, X. Xin, S. Guo, Y. Zhang, L. Yang, B. Wang, X. Li, Chem. Eng. J. 384 (2020) 123337.
[164] T. Shi, W. Yan, Z. Zhang, L. Meng, C. Liu, X. Yan, Catal. Lett. 154 (2024) 42–49.